Raman Characterization of Polymer Formation

-First Step to Self-Healing Polymer Coatings Studies-

DISSERTATION

Zur Erlangung des akademischen Grades

doctor rerum naturalium (Dr. Rer. Nat.)

vorgelegt dem Rat der Chemisch-Geowissenschaftlichen Fakultät der

Friedrich- Schiller- Universität Jena

von **M. Sc. Simona Vasiliu**

Geboren am 06 März 1986 in Vatra-Dornei, Rumänien

Gutachter:

1. ....
   ....
   ....

2. ....
   ....
   ....

Tag der öffentlichen Verteidigung: ....

Contents

"Prin muncă şi stăruinţă, vei ajunge la dorinţă."

Introduction

"People often say that motivation doesn't last. Well, neither does bathing – that's why we recommend it daily."-Zig Ziglar

Self-healing materials are the solution to the damage of a material, offering long-lifetime material structures, through the combined work of the scientific research and industry application developments. [1-3] In principle all the materials available for precise applications have features that are designed to complete their functions. More and more structures are being improved either in a singular design, considering only one type of material, or joining different kinds of materials and building a new reinforced structure, that can be easily used in other conditions as it used to be before the blending.

On the other hand the self-healing can be defined as „the capability of a certain material to repair/heal/recover damages in an automatic and autonomous way, or better yet without additional intervention". [4] Considering these definitions of self-healing it can undoubtedly be stated that the inspirational source are biological systems (as presented in **Figure I.1**). Several assemblies of self-healing structures have been presented in the scientific literature [5-7] and the resemblance to the nature-inspired structure is obvious.

Similarly to the structure inspiration, the working mechanism is a great example of natural functionalities. For instance, inherent responses can include simple rebuilding of the structures, restoring mechanical properties, as well as other functional characteristics necessary for the full system to work at a complete capacity. The regeneration of the natural environment offers the explanations needed for the definitions for the healing process.

Accidents like broken bones are solved with simple replacements made of materials that due to their designs are biocompatible with the human body. They don't interfere with the healing of the human organism, they are present just to support the displacement, to replace the missing part, or simply to make the connection between the injured parts. Although these types of injuries need external and technological interventions, the nature-inspired systems exhibit actions based on the biological responses that will not require additional assistance when healing the damage. For instance, the same path of independent reactions can be

demonstrated for an injury like a skin cut (see **Figure I.1**): the damage itself will trigger the organism's response, initiating the healing process.
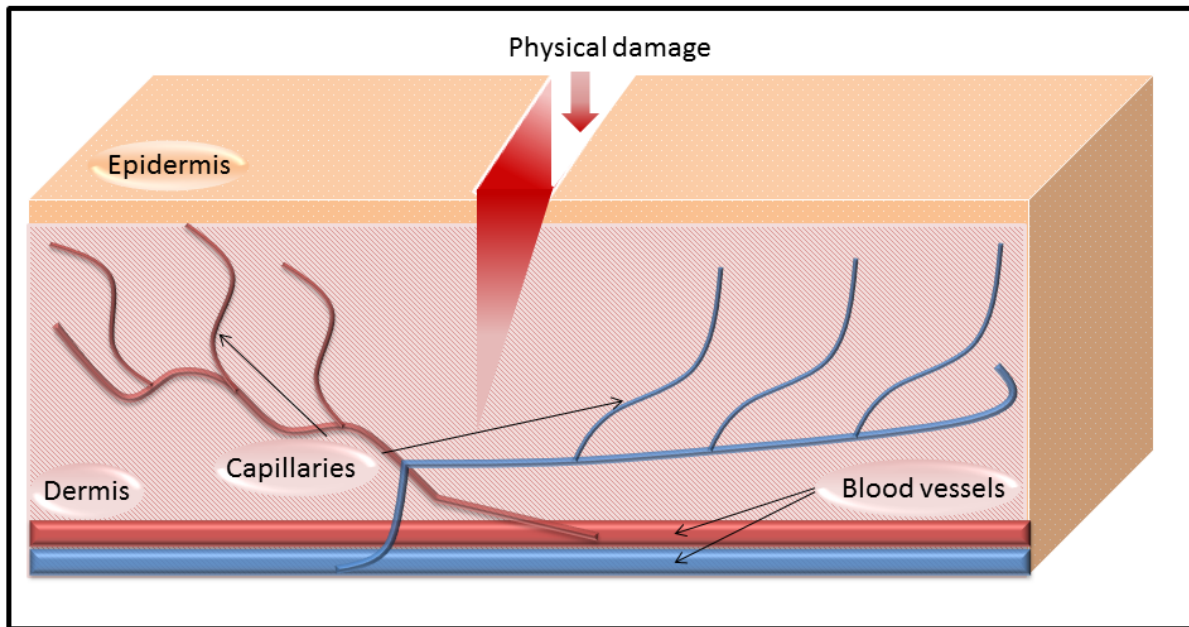
Figure I.1 *This image illustrates a skin cut and represents the most expressive example that provides the necessary inspiration for the self-healing mechanism.*

One simple example of nature inspiring-model is an injury on surface of the skin of an organism (shown in **Figure I.1**) where the supporting self-healing system is represented by the blood-flow send as a response to the inflicted damage. Here the bloodstream helps to recover and heal the occurred damages, through the blood-clotting. A straightforward idea is that biological influence helped and provided the necessary inspiration (structures containing capsules or vascular matrix) for the development of this type of smart materials. The basic steps of the self-healing process are associated with the actions of the surrounding nature, considering also the stages that complete the evolution of the mechanism.

For example, inspired from the behavior of mussel byssus a research study [8] investigated and developed a self-healing material based on reversible metal-ligand interaction. [9, 10] Additionally, metallopolymers (the mussel inspired metal-binding) were developed and even if the re-structuring process is present with moderate self-healing features, still no measurable evaluation was possible. [11]

Keeping in mind biological (skin cut) example [12, 13] one can expand now these facts and imagine being capable to apply similar theories in other activities. If the biological systems can heal themselves, which could improve their lives, which could also lengthen their

lifetime, and could also restore functionalities and properties lost upon injury, then the advantages provided for the materials science and/or for the industrial engineering would be highly appreciated.

The definition of a self-healing material does not specify in which range the material will regain functionality, or which features of properties will be affected and how will they be restored. Therefore the class of self-healing materials and their response to damage or how the self-healing process will take place, represents a branch of research strongly defined.

In the case of coating materials several designs have been investigated. [14] Major classifications have been made, in order to find the appropriate combinations between the materials prone to corrosion, and the coating materials.

From a chemical point of view self-healing materials are rather complex systems covering both anorganic (self-healing cement[15]) and organic [16, 17]. Most of the self-healing materials developed up to now are organic polymers and therefore these particular chemical compounds are of a high interest for the development of new materials.

Building and developing new materials is a stage followed by improving the analytical methods that are employed for the characterization of such materials in order to find specific features. [18, 19] To this extent, particular analytical methods have been employed for the characterization of self-healing polymer coatings, but mainly for assessing the macroscopic properties. To monitor the healing efficiency complex analysis of the mechanical properties was used.[20] Visualizing of the process that takes place in these novel materials was possible with the use of scanning electron microscopy or X-ray tomography. [21-23]

A complete image of the functionality and developed processes of these type of materials needs approaches from both macroscopic level, but as well a deeper view of the molecular behavior. Spectroscopic techniques (NMR, IR, Raman spectroscopy) [24, 25] are well suited to perform analyses at a molecular level. In this direction it can be mentioned that the observed complete regions of a complex polymer sample did not provide distinctive information regarding the possible molecular processes.

In this context, Raman spectroscopy has proven to be a useful tool for polymer investigations [26-28] obtaining detailed information about the properties and the molecular structure. Although, spectroscopic investigations of the self-healing polymers have been presented [29], the monomers were not the target of the observations, but the complete polymer sample. On this matter, the aim of this study was to illustrate the capability of Raman spectroscopy to analyze and characterize the formation and the processes that take place in novel polymers as

a primal step for the investigations of the self-healing materials, particularly for the self-repairing polymer coatings.

In this work the capability of Raman spectroscopy to characterize the process of self-healing in novel polymers will be presented. The spectroscopic approach allows us to identify marker bands for an individual chemical compounds taking part in the reaction and, by that, provides means to follow the reaction with temporal, and in general also spatial resolution. While the experiments presented here deal with an in situ spectroscopic study of the chemical reaction underlying the self-healing in a polymer coating, they form the basis for subsequent investigations on actual material properties, which are to follow in a conceptually later step.

 Due to the complexity of the investigated molecules (such as polymers) a precise assignment of the Raman bands can be a difficult task. Therefore, a detailed assignment of the Raman bands by means of the theoretically calculated spectra is required.

The next sections of the present work will at first introduce some theoretical aspects and classifications of self-healing materials and the involved chemical reactions, as well as a brief characterization of the corresponding self-healing mechanisms. The following chapter containing experimental details will refer to the description of the Raman micro-spectroscopy setup used for the polymer sample investigations, along with the integration of the analyzed samples classified, according to the chemical reactions, in two categories. Additionally, complete discussions of the analyzed samples together with the results of different experiments showing the behavior of the chemical reactions by revealing the targeted Raman marker bands will be presented. At this point, the analysis of the "click"- reaction will show the temporal profile of the azide-alkyne cycloaddition, but only after demonstrating the influence of the individual chemical components. Following the same observational trend, the investigated samples based on the Diels-Alder chemistry will present a specific behavior during temperature treatment, concluded with the clarification of polymer formation. All the analysis will carefully relate to literature capable to support the provided information and introducing the concluding remarks as common chapter. In the last parts of the work at hand one can have a complete and merged overview of the Raman investigations of both chemical reactions while supporting the self-healing mechanism.

2. Theory

In this chapter the focus of the description will target mainly a general characterization of the self-healing materials, as well as a presentation of the most important industrial and also research applications. Along with the presented type of self-healing materials additional link shall be made towards the employed mechanisms (as a general purpose, or specifically for this study). The topic will shift later on towards general theoretical details of Raman spectroscopy, directed to the polymer investigations.

Smart materials are defined as systems which can repair themselves without external intervention and these will respond to a stimulus in general with a single expected action. Normal materials have a limited possible responses (the difference between the mechanisms) - also as compared to the *intelligent materials* which are designed strictly to respond to a stimulus with an accurate response and with different probable actions. [6]

The ability to respond to a discontinuity of a system in such a way that the structure will re-gain its initial functions, can be defined as self-repairing and can hardly be found within artificial structures. It is noticeable and valid to express that self-healing materials are smart materials since a system with an incorporated feedback can respond appropriately to its environment. [30, 31]

The above description shows a new development of the material science, the approaches used to describe the novel materials and their possible responses to damage. To this extent, the next section will contain a detailed review of self-healing materials in particular.

Possible strategies for damage monitoring involve the hypothesis of the fracture being present at a microscopic scale when the damage cannot be evaluated properly from the beginning, but once it can be noticed then ruptures are already formed and they can be slowed, but can't be stopped from propagating. Thus the progress in the material engineering is constantly aiming towards directions like *damage prevention* rather than *damage management*. [2] The difference between these two approaches is that *damage prevention* paradigm represents the characteristic of materials that prolong their lifetime and postpone any fractures and damage with the help of their design, but they have no ability to repair the disruption. When referring to the *damage management* concept, one has to define the type of materials where the design has incorporated characteristic that will trigger an appropriate response, during use, when damage occurs in within the system. This response will be able to repair the damage, rebuild the structure and, of course, prevent other propagation or following rupture results. [2]

As mentioned before, the healing of human organism (i.e. a skin cut) takes place as soon the system is in full knowledge of the rupture, and it can also be added that the damage itself has triggered the healing process, since in this case the blood flow will immediately be send to the wound filling up the newly created space, re-structuring the broken bonds, as well as their functionalities. With the help of the nutrients (like glucose, amino-acids, fatty acids) carried by the blood plasma the wounded site will be healed and protected until the process reaches completion.

Step by step the design inspired by the natural-model, describes the main characteristic of self-healing material: triggering an appropriate response in case of sudden failure. This main feature is in charge of tracking the damage and initiating the mechanism that will send the stored material in order to fill the emerged crack, or simply to be able to re-arrange the distorted structure. The next step is to create the flowing response of the material which must have a different construction in order to perform its capacity of moving through the entire system and reaching the damage site, where with the help of several offered chemical reactions, a response can re-arrange the disrupted components. Therefore, the new materials should inherently construct a structure with a solid and rigid main matrix containing also a mobile healing component (agent).

Introducing the healing agents into the rigid matrix through some microscaled containers is most desired approach to be used (see **Figure 2.2**). Certainly, the optimal strategy was researched so that the containers can be dissipated into the entire volume of the rigid matrix-material. Therefore, when the damage occurs, e.g. a simple cut, the content of these micro-containers will flow out, and in the contact with the rest of the matrix a chemical reaction will take place favoring the completion of the self-healing process.

In the above situation the damage itself can trigger the self-healing mechanism. The list of factors that can initiate a self-repairing mechanism is however manifold: light, increased temperature, UV-light, different types of pressure are among the available parameters that can participate in the self-healing process.

2.1.1 Types of self-healing materials

This section is dedicated to a detailed presentation of the types of the self-healing materials. In the **Figure 2.1** one can observe a list of novel materials that the material engineering and the research studies have developed by now as smart materials. Example of systems that can support the improvement of polymers (as well as polymer coatings, which is the consequent

subject of this work), concrete and asphalt, metals, structural ceramics, or even optical materials are presented.
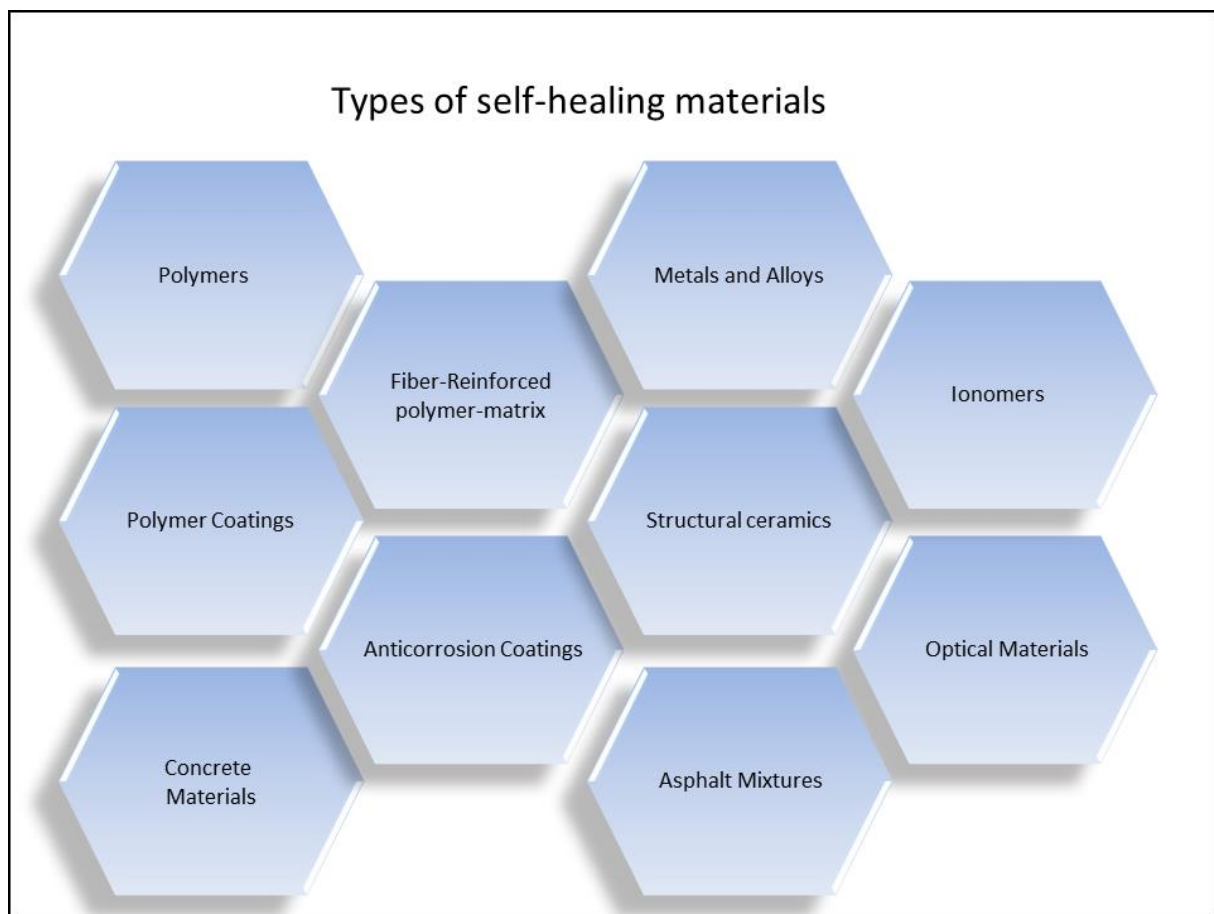
Figure 2.1 *The current figure offers a short schematic view of the possibilities offered by the self-healing material branch.*

Following the above illustrated classification of self-healing materials, in the next lines a short description of a few examples shall be presented. Starting with a material like **concrete** according to the one of the most cited works, "Self-Healing Materials" [2] , similar behaviors of self-healing materials have been employed ever since the Roman Empire times, having as an example the mortar used in building construction or other frameworks. Thus, combining a bulk structure-material with living organisms (bacteria) became a completely viable process [32-34], in which case a mineral-producing bacteria was attached to the structure of a new-developed concrete. [35-37] This material is defined as a product that has the biological ability to produce limestone, necessary for crack-healing. The bacteria employed for this type on self-healing concrete is the genus *Bacillus* together with the calcium-nutrient calcium lactate plus phosphorus and nitrogen. The trigger for this self-healing is represented by the water infiltration, where the spores of the bacteria will germinate in contact with the water

and the bacteria will be activated. Subsequently the bacteria will initiate feeding on the calcium lactate, furthermore transforming into insoluble limestone. The limestone will be immobilized on the crack surface sealing it up. It can be observed that this healing has a strong resemblance to the human broken bones, where the healing occurs with osteoblast cells that mineralize to restructure the bone. Additionally, prior to the development of this material, several types of bacteria were tested in order to establish which one will survive the best in within the concrete structure, and the genus *Bacillus* able to present a stand-by state for longer than any other type. [38] Close to this material category, the cementitious composites present a concept where the embedded capsules into the composite structure have an oil core and a silica gel shell and they would contain a methyl methacrylate monomer and triethylborane as a healing agent. The capsules, within micrometric scale, will afterwards be distributed in the fresh cement mortar. As mentioned before, the healing in case of micro-encapsulated containers occurs when a rupture-damage takes place. The rupture stress will break the micro-capsules releasing the healing agent, which will fill the cracks. Due to the contact between the healing agent and the catalyst, the polymerization is initiated to re-bond the crack surfaces. [39]

Another category of materials that has a great success in the branch of self-healing materials is represented by the **asphalt** composites, where asphalt mastic has been investigated and the characterization results showed that the self-healing properties of this material involve temperature treatment or by surface wetting. Several types of designs are available, i.e. asphalt mortar containing fibers and fillers or asphalt mastic and porous asphalt concrete. [15, 40, 41] Self-healing asphalt is a material that has been employed in industrial application, for instance in building some motorways sections in The Netherlands.

In the case of **metal**-based materials, due to the metallic atoms being bonded in rigid manner, they will have low diffusion rates and small volumes. Therefore, it has to be mentioned that it's even more demanding to develop a strategy for the self-healing metal composite. The work approaches in this direction are conditioned by the construction of the metallic systems. One example is presented in the study of aluminium alloys using porous powder and tuning the precipitation phenomenon. Additionally, self-healing in metals is demonstrated to be possible through the adjusting of the precipitations processes. [42]

One of the most applicable discoveries and developments has been made in the domain of **polymers**, which have been proven to conveniently be used on the subject of self-healing

polymers thanks to not such a rigid structure. Also polymeric materials represent materials that are easier to be developed in a laboratory, in safe conditions where there is no need for large devices to perform the tests compared to the analysis made in the case of concrete, cement or asphalt.

Since the healing process of these smart materials is mainly based on molecular reactions or on structural changes, it is more likely to work and develop new designs and structures suitable for polymeric materials. Such a design example can be noticed in the below lines, in **Figure 2.2**, where the necessary microscaled containers that have to be embedded can be projected with different shapes and volumes, and they are not in danger of being crushed by the main structure, compared to the case of asphalt and concrete constructions.
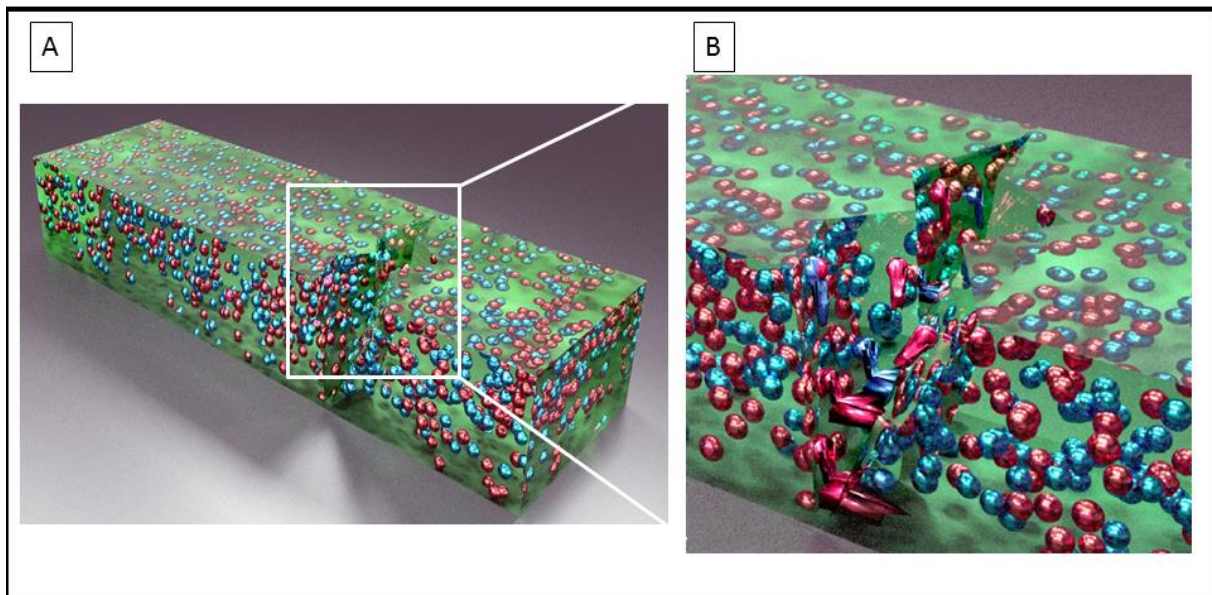
Figure 2.2 *Design of the self-healing materials- this image captures the functionality of the self-healing polymer coatings based on the micro-capsules embedded into the polymer matrix system. One can observe that the damage itself will trigger the self-healing process. Panel A represents the possible damage occurred in within the polymer structure, while in panel B one can find a schematic view of the self-healing process that takes place when the ruptured capsules will release the healing agent, re-structuring the displacement of the system.*
(adaptation to reference [43])

The design of material involves the presence of an embedded capsules system into the polymer matrix. This approach is one of the most utilized and described in previous literature [44], but does not represent the only employed design for the development of such structures. Several parameters can be tuned for a better outcome of the material functionality. In this

direction it has to be mentioned that the size of the capsules can vary from 200 μm to 20 μm, and also that the most common shape used for the capsules is spherical. On this basis the research works on describing also another system, similar to the microencapsulation, but instead of spherical capsules the authors M. Motuku et al. use a tubular shape [45] where they can store the liquid self-healing agent. These kind of system are called self-healing micro-vascular, and the healing agents are delivered to the damage by an embedded vascular network, that can have different dimensional connectivity (1D, 2D, 3D). Regarding the last mentioned healing agent delivery system, it can be observed the similarity to a fully bio-inspired system, since this type resembles the bloodstream of a mammal organism.

A large variety of healing agents has been employed for the use of polymer capsules content. For instance, one option was an *endo-* dicyclopentadiene (*endo*-DCPD) and 5-ethylidene-2-norbornene (ENB) with an additional fluorescent dye, were incorporated into a melamine-urea-formaldehyde shell by *in situ* polymerization, where the diameter of the capsules was approximately ~80 and ~50 μm. Others have used micro-capsules (with an average size of 100 μm) containing epoxy resin, produced with *in situ* polymerization, and the urea-formaldehyde based shell was formed over the epoxy resin bead. In the same context of embedding micro-capsules into the polymer matrix, other experiments have used the *in situ* healing compound encapsulation method. [46]

This section was able to identify several developments in the materials engineering and as well in the material research, and a classification of the most employed materials (in the domain of self-healing materials) was made. Types of self-healing agents and the shape of the pre-embedded micro-containers were shortly analyzed, with scope of offering a deeper understanding of the cornerstone for the utilized chemistries.
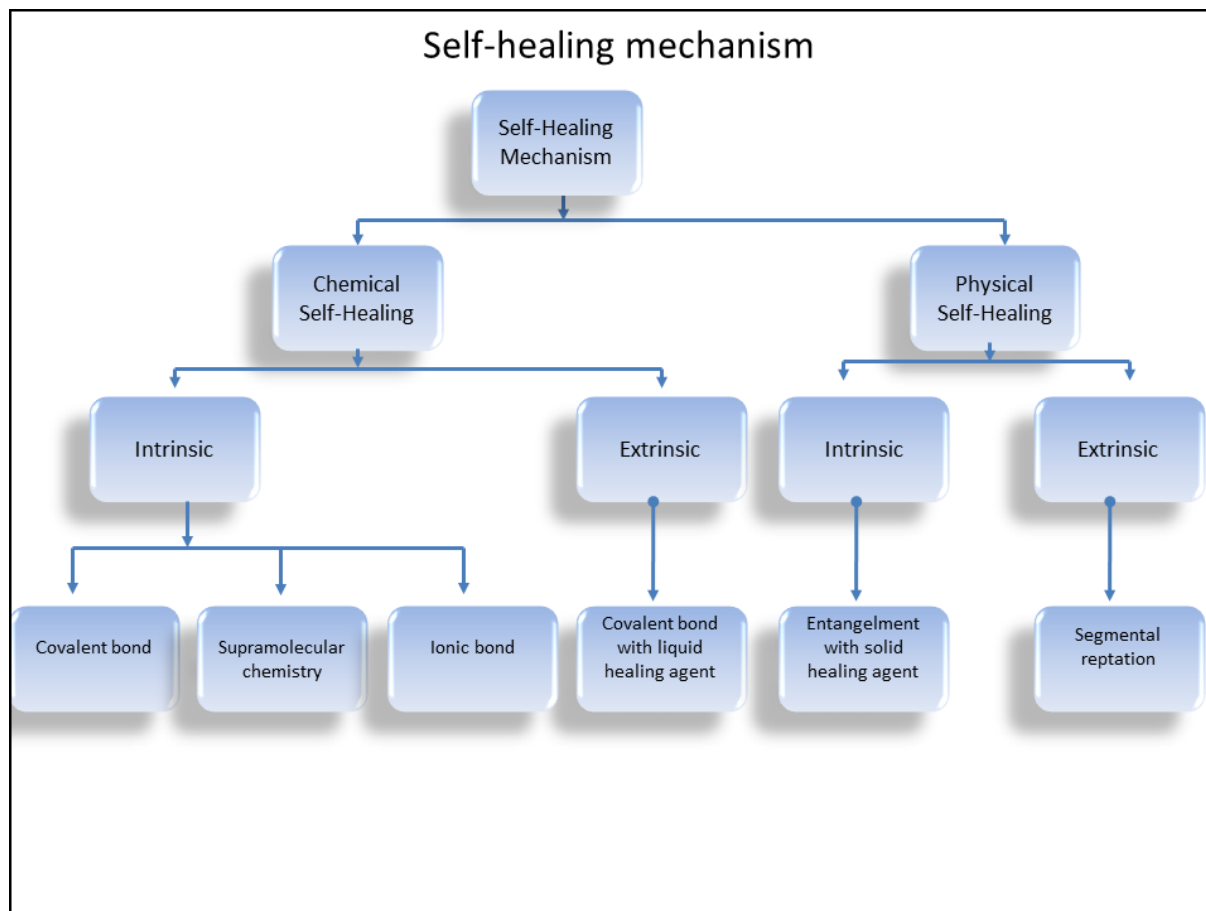
2.1.2 Types of self-healing mechanisms

An important aspect during the presentation of the self-healing mechanism refers to the repetition of the repairing cycle. One of the most efficient strategies is to develop a mechanism that could apply to materials that can accomplish an unlimited number of self-healing cycles, so that the activity can continuously and constantly work, maintaining a high performance. A clear difference can be stated between the definition of independent (*autonomous*) self-healing mechanism and the definition of dependent (*non-autonomous*) version of the self-healing mechanism. The different types of structures offer simple point of view of nature inspiration, but the cornerstone of the actual functionality of the self-healing

materials is mainly based on the self-healing mechanism that take place as an auto-repairment.

The **autonomous** self-healing mechanism (from greek *autonomia*) refers to the self-contained, self-sufficient mechanism, where the damage itself represents the trigger for the self-healing. More in detail was presented previously in the case of the rupture of the pre-embedded microcapsules, where the healing agent from the capsules will flow into the polymer matrix and a chemical reaction will occur in the presence of the catalyst (also pre-embedded). On the other hand the **non-autonomous** version of the self-healing mechanism is by definition dependent on the existence of additional external factors that will trigger the self-healing mechanism. To exemplify, various studies in this domain have established a rich choice of characteristic elements that can initiate the self-healing mechanism, some of them being increased temperature, UV light, pressure and others. [47, 48]

Another approach that can define the healing features of the self-repair mechanism is illustrated in **Figure 2.3**. In this figure it is to be observed a distinction between the chemical and the physical aspect of a self-healing process. Each one of the two approaches, chemical and physical, has in turn two other types of response mechanisms: an **intrinsic** and an **extrinsic** character. [49]

Figure 2.3 *Short schematic view of the classification of the self-healing mechanisms.*

The above comparison provides us with the several types of self-healing, as well as bringing a more detailed and accurate overview of the chemistry involved into the processes. At the same time this clarification represents a starting point for the introduction of the steps involved with the self-healing mechanism.

When referring to the **extrinsic** mechanism one can simply understand that additional and external intervention is required, therefore here the material design contains separate structure where the healing agent is stored. This is the well described structure of the embedded capsules or the vascular system. [50, 51]

In the next paragraph one can observe a few examples that can demonstrate the clear difference between the two types (chemical and physical) of self-healing mechanism, presented in **Figure 2.3**. When referring to the behavior of the **chemical self-healing** mechanism, it comes to be detailed for instance, why the covalent bonding is one of the best choices when designing a self-healing system. The *exo* or *endo* formation between a diene (i.e. furan) and a dienophile entity (maleimide) is the first step to a self-healing mechanism.

The reaction here, Diels-Alder and *retro-* Diels-Alder, was employed in systems like polystyrene, polyamides, and epoxies. [52] On the other hand the **supramolecular chemistry** involves characteristic features (sensitivity, reversibility and directionality) that make this a good option for self-healing processes. In this category of the supramolecular chemistry one can find systems like the hydrogen bonding (weak non-covalent interaction), which have been used as foundation for the ureido-pyrimidinone (Upy) derivates, or with the help of click chemistry, being part of the polyisobutylene structure [53], moreover being observed in poly(vinyl alcohol)hydrogels [54]. The self-healing behavior of **ionic bond** interaction has been intensively studied, for instance in polymers like poly(ethylene-*co*-methacrylic acid-EMAA) and polyethylene-*g*-poly(hexylmethacrylate- EHMA) [55, 56]. [57]

Physical self-healing refers actually to a physico-chemical healing due to the fact that the healing depends explicitly on the chemistry of the material system, but also on the specific physical principles like welding and swelling. [3]

The segmental *reptation* with entanglement of the solid self-healing agents is part of the classification of the self-healing materials, when physical self-healing mechanism is exhibited. In the classical sense *reptation* if defined as being the thermal motion of a complex long and linear entangled macromolecules in polymer melts or other polymer solutions. The movement of the polymer suggests a slithering of the polymers one to another.

In other words the *reptation* theory presents the effect of the polymer chains entanglements in reference to the relationship between the molecular mass and the chain relaxation time, τ. The approach focuses on the presumption that the polymer chain will occupy the tube with L length, where the *reptation* motion might be possible. Approximating a time scale of τ, an all-encompassing move may be described. Therefore the mobility through the tube can be defined as $\mu_{tube}=v/f$, in this case the velocity v of the polymer chain depends on the exhibited force f, necessary to pull the chain trough the motion. [58, 59]

The *reptation* feature, an important characteristic polymer property, is often used to declare the quantification of the physical self-healing mechanism type. [58] The above definition of this polymer attribute (here stated in a general form) described at the same time the motion that the polymer must perform in order to be found a position in which the self-healing mechanism could be triggered.

As particular case in the next lines the *autonomous extrinsic self-healing mechanism* (shown in **Figure 2.4**) shall be presented, along with the basic steps that occur during this type of mechanism (polymer samples based on azide-alkyne cycloaddition).
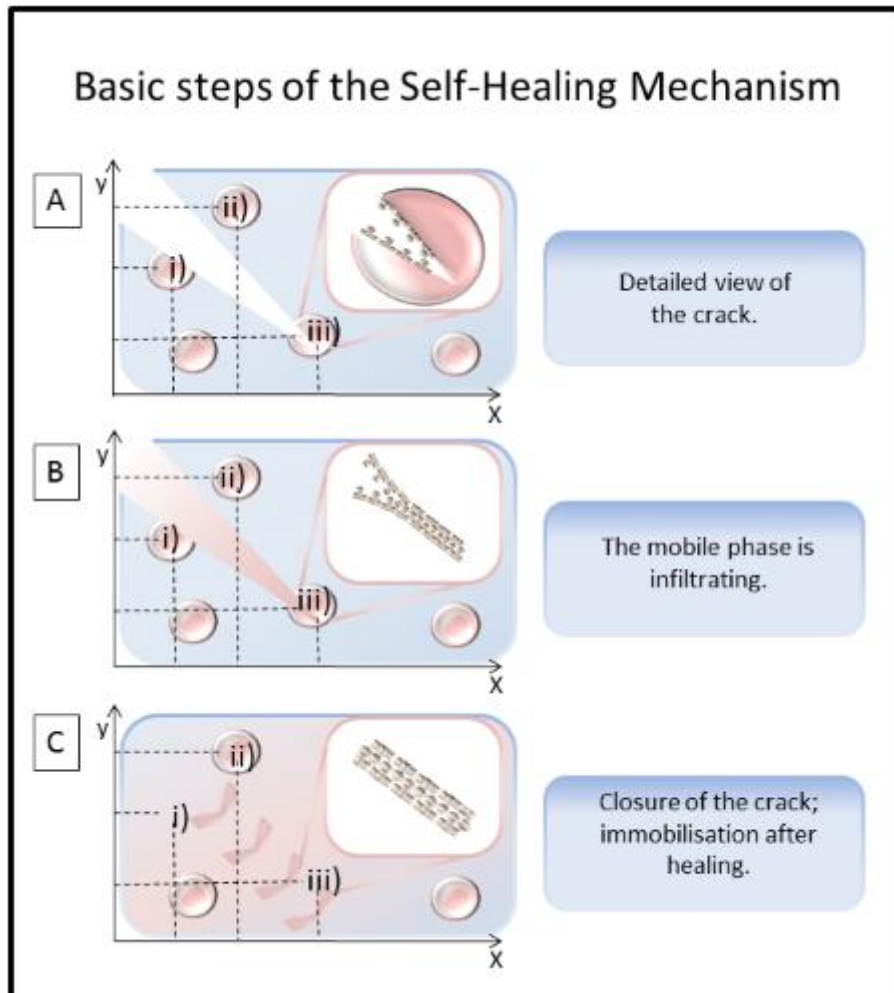
Figure 2.4 *The figure shows the damage event occurrence and the principle according to which the self-healing material (pre-embedded microcapsules) works. Also the basic steps of the self-healing mechanism present here a statistical behavior of the microcapsules, when a damage stress disrupts the natural functions of the material.*

In panel A of **Figure 2.4** the first step of the self-healing mechanism shows the presence of the damage stress. Here one can observe a detailed view of the crack which, as previously defined, represents the first step of a healing process, here demonstrating the autonomous mechanism by triggering the self-healing mechanism itself.

On the other hand the Cartesian coordinate system has been attached in order to demonstrate the possible behavior of the pre-embedded microcapsules during the damage event. The first step of the self-healing mechanism illustrates the choice of 3 different microcapsules, found in dissimilar established positions i), ii) and iii).

After the crack damage has destroyed the material system, the second step of the self-healing mechanism takes place and in this case in panel B of **Figure 2.4** it is shown the initiation of the mobile phase, since the crack damage has ruptured the microcapsules and the liquid self-healing agent bursts out, flowing into the polymer matrix.

At the same time the second basic self-healing step of the process it's represented with the coordinate system in order to follow the previously established positions of the microcapsules. One can easily noticed that the capsules that will be affected by the crack damage are assigned to i) and iii) positions of the coordinate system, while the ii) established position represents the possible behavior of a capsule that does not meet the route of the crack-damage.

Enclosing the overview of the classical self-healing mechanism steps, the third level of the repair behavior is shown in panel C, where after the immobilization of the material system, the re-structuring of the system is visible, while the crack closure is represented as healed zone, but still exhibiting itself with a scared surface representation.

Comparing now the influence of this final level of healing, in panel C the immobilization of the repaired structure shows the positions established by the coordinate system with the lost target of the microcapsules or, a far much better definition, the consumption or the incorporation of the liquid self-healing agent into the material system. Still this presentation approach shows that the capsule corresponding to the ii) position is yet present, and undamaged, since the position was not on the path of the crack-like damage.

The **intrinsic** [60] mechanism approach converges to an ideal system healing exhibits self-healing properties from the beginning of the formation of the structure. Here the healing agents are attached to the polymer matrix, without the needed presence of an additional catalyst. On the other hand it has to be clarified that the self-healing agents are here represented by reversible crosslinks, which are molecular interactions that can re-structure following destruction rupture. Types of the chemical bonds that can provide such a

mechanism, are examples like the Diels-Alder and retro-Diels-Alder reaction [61, 62], hydrogen bonding [63], ionic bonds [55, 56], π-π interactions [17, 64, 65]. [8, 57]

The basic features of the *non-autonomous intrinsic self-repairing mechanism*, that represent the foundation of the investigated sample based on the Diels-Alder reaction is represented in **Figure 2.5** along with a short description of the active followed steps involved in the mechanism's occurrence. A close insight into the components that take part at the reaction is also shown (**Figure 2.5**, insight **c1)**).
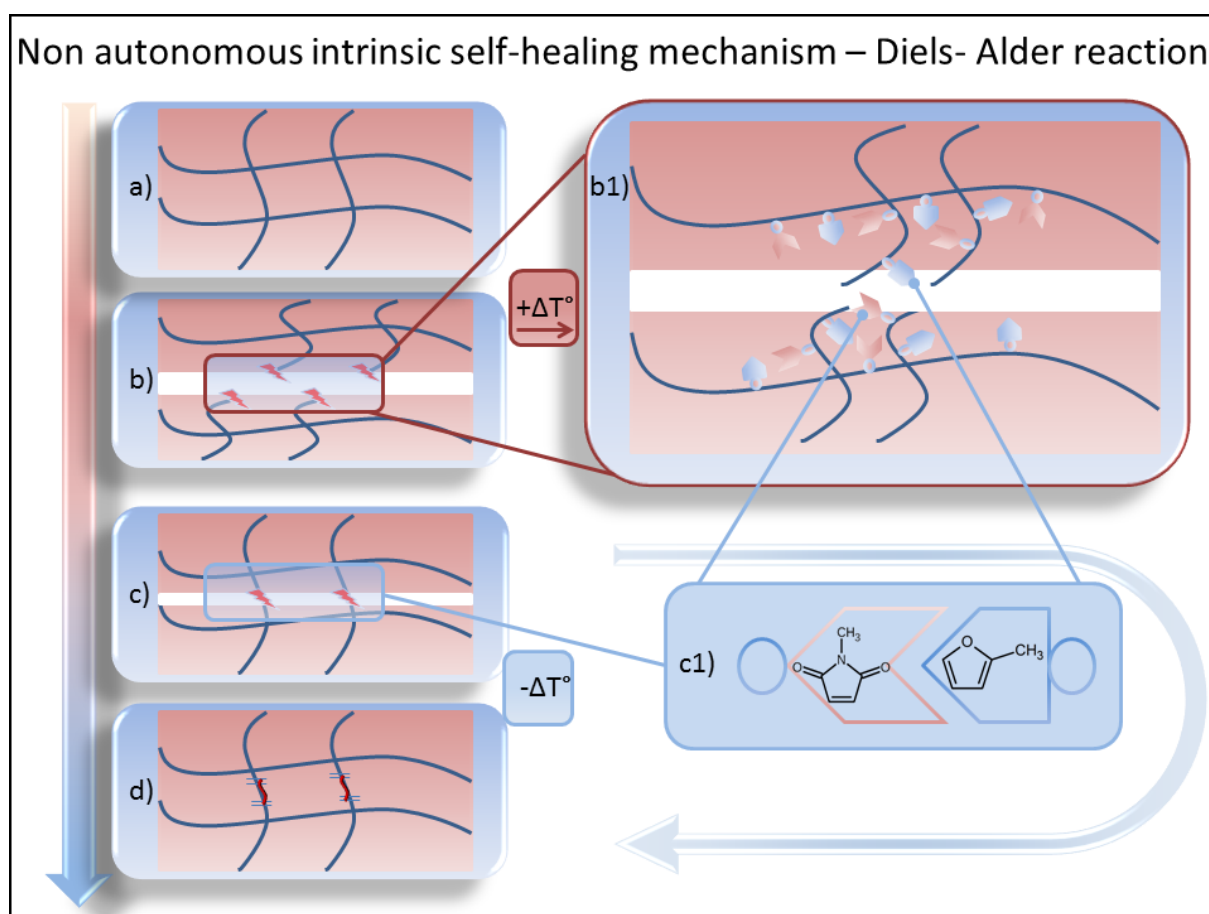
Figure 2.5 *Image that presents the basic steps of the self-healing intrinsic mechanism.*

The panel **a)** of the **Figure 2.5** shows the initial-intact state of the material, while furthermore panel **b)** presents the damage occurrence, therefore disrupting the functionality of the structure. As mentioned before temperature treatment will be applied in order to create the pre-requisite "mobile" phase of the self-healing mechanism, schematically pre-viewed in **b1)** inset picture where one can take a closer look at the self-healing agents (crosslinking agents of the Diels-Alder cycloaddition, furan and maleimide) connected to the main structure. Upon cooling the two crosslinking agents will restructure the system as shown in step **c)**, but as well

in the **c1)** inset, where the two agents are able to re-attach to the polymer matrix, resulting with the bond reformation and the crack closure, as presented in step **d)**.

Independently of the nature of the material, from a functional point of view it's not only necessary to restore the mechanical material properties, but also to decode the internal molecular behavior accountable for the self-healing mechanism. Nonetheless the most important aspect of all is the analysis of the basic steps of the self-healing: establishing the post-damage modifications in within the molecular structure, describing the occurrence of the *mobile phase* and the influence of the pre-designed chemical structure, and in the end the immobilization of the *mobile phase* together with the re-arrangement of the damaged material structure.

In the next section one will find a complex description of the two main chemical reactions used in this study for the investigations of polymer samples. Principal theoretical details for each reaction, as well short introduction of the main components will be discussed. Starting with the azide-alkyne cycloaddition and following with basic theory of Diels-Alder reaction, one can also find some short presentation of possible examples and applications of these chemical reactions.

2.2.1 Reaction 1 ● Azide-Alkyne cycloaddition

Azide-alkyne copper based catalyst reaction represents one of the most popular reactions using the click-chemistry concept. Furthermore the „click" chemistry defines the elucidation of pairs of functional groups able to rapidly and selectively participate in a reaction, in any mild or aqueous conditions. A criterion step during the click-chemistry functionality is represented by the presence of compatible-click functional groups A and B that will enable the formation of a stable conjugated click-activated molecule. Moreover, it is generally known that the click-chemistry prefers simple reaction conditions, as well using the available starting materials, no additional solvent use.

On the other hand when K. B. Sharpless [66] introduced the term of click-chemistry, it was a notion used to present reaction wide in scope, high yielding, creating byproducts that are stereospecific. Several other chemical reactions have presented themselves to satisfy these criteria. [66] In the case of the azide-alkyne cycloaddition many of the starting monosubstituted alkynes and the organic azides are commercially available, or they can easily be synthesized large-scale of functional groups. Still the original version of the thermal

Huisgen 1,3-dipolar cycloaddition [67] of alkynes to azides, must take place at high temperatures, which contravene with the previously established definition of click-chemistry. Therefore to this matter, the classic version of the 1,3-dipolar cycloaddition does not fit the equivalence of a valid click-chemistry reaction. The variant in which a copper catalyst participate to the reaction, demonstrates a different mechanism according to which the reaction can take place in aqueous environments, and most important at room temperature. Furthermore, while the classic Huisgen 1,3-dipolar cycloaddition offers mixtures of regioisomers, the copper catalyzed reaction variant will provide the synthesis of 1,4-disubstituted regioisomers. For a better understanding of the click-chemistry of the azide-alkyne cycloaddition, one should firstly follow the classical mechanism of the Huisgen reaction. [68]

Due to no need for constant addition of healing agents (see the Diels-Alder reaction) the main advantage of such cycloadditions while developing self-healing polymers, is the presence of a large number of repetitions of the repairment process.[69] Thus when determining types of cycloadditions the factors to be taken into account are the number of the σ-bonds formed or the classification can be made considering the size of the future-formed ring. Most likely, with the help of two reactants, and at the cost of two π-bonds, a new cyclic compound will be formed generating two σ-bonds. [70] On the same basis kinetics and mechanism of the 1,3-dipolar cycloaddition were investigated for detailed understanding of the system. [71]

While the Cu(I) catalyzed Huisgen reaction provides the selective occurrence of the 1,4-triazole, the classic version of the thermally triggered Huisgen cycloaddition will result in a close 1:1 mixture off 1,4- and 1,5-triazole stereoisomers. In the work of J. E. Moses and A. D. Moorhouse [72], the click-chemistry receives new directions by being empowered to submit to several different domains, where the vast range of applications make use of the click-reactions. To convey to an illustration of the intersection of chemistry with biology [73], medicine [72, 74, 75], modifications of proteins and nucleic acids by attaching ligands, radioisotopes, or by simply fusing multiple proteins together, and here this process is defined as bioconjugation. [74]

Click-chemistry is a very important synthesis path for the development of new self-healing materials. Here the research has proven efficiency in the case of polymer synthesis, where for instance polymers with strong potential for medical applications with alkyne derived polymer backbone, followed by the azido-sugar residues, were blended together in the presence of the

Cu(I) catalyst to perform a Huisgen cycloaddition (similar approaches for organogels [76], nanotechnologies [77], self-assembled monolayers [78]). [79]

The self-repairing system based on the pre-embedment of microcapsules can exploit the self-healing mechanism with the help of the azide-alkyne "click" reaction. [80, 81] Previously in this work it has been illustrated (see **Figure 2.4**) that the self-healing mechanism for this kind of system will be triggered by the damage itself. Thus, the only necessary step is damage occurrence at the level of the microcapsules structure, initiating the burst of the liquid self-healing agent that in the presence of the catalyst will trigger the azide-alkyne cycloaddition. The study at hand presents an azide-alkyne copper(I)-catalyzed cycloaddition-reaction. The self-healing agent contained by the microcapsules is a polymeric or oligomeric based reactant to initiate self-healing, i.e., three-arm star polymers, together with a Cu(I) catalyst. [82-84] The scientific research literature [19, 85] in this domain notes that the auto-acceleration of the self-repairing reaction exhibits a higher reaction rate of the mono-, di-, and tri substituted alkynes with a visible advancement assignable to the occurrence of triazole-based Cu(I)-clusters, behaving like ligands for active copper-ion, therefore accelerating the crosslinking reaction.

2.2.2 Reaction 2 ● Diels-Alder cycloaddition

The Diels-Alder cycloaddition [86] is an organic reaction that has the capacity of forming carbon-carbon, carbon-heteroatoms and heteroatom-heteroatom bonds. In the classical sense of definition the Diels-Alder reaction is a cycloaddition between a conjugated diene and a dienophile, the last one has at least one π bond. The reversibility of the *hetero-Diels-Alder* reaction becomes possible under the influence of different factors. The Diels-Alder reaction presents with both intermolecular and intramolecular features. Going back to the components of the reaction, it must be defined that the conjugated diene will supply the double bonds. Also, there is a demonstrated efficiency of cyclic dienes when compared to the reactivity of the open chain types.[87]

The Diels-Alder reaction is also reversible and the route of the cycloaddition is supported due to the replacement of the two σ bonds with new π bonds. This cycloreversion occurs when the diene or a dienophile become remarkable stable molecules (e.g. aromatic rings formation, or nitrogen, carbon dioxide, acetylene, etc.), or in the case one of these components can be separate or consumed in an additional reaction. Additionally, the *retro Diels-Alder* cycloaddition has a prerequisite condition of high temperature so that overcomes the

relatively high activation barrier of the cycloreversion. At the same time the retro Diels-Alder approach is useful in organic synthesis to protect a double bond or to cover a diene fracture-part.[88] [89] [90] [91-93]

In the course of this work the Diels-Alder cycloaddition was employed for the polymer formation, where the functionality of the self-healing mechanism was displayed in **Figure 2.5**, along with a complete description of the participation of the two crosslinking agent furan and maleimide (see **Figure 2.5 c1)**).

2.3 Raman Spectroscopy

Raman spectroscopy is an investigation tool that provides sensitivity and specificity necessary for understanding the structural modifications in molecules and materials. The leading focus of the work at hand will be represented by the investigations performed using Raman micro-spectroscopy in which case Raman scattering is integrated to a light microscopy system.

Raman scattering or the Raman effect [94] represents the inelastic scattering of a photon after the interaction of an electromagnetic field with a molecular system. [8] [95] The distortion of the electron cloud constitutes the „virtual state" level as a short-lived state of the molecule. The stability of the molecule in this level will change as the molecule will return to a lower level as a consequence of photon radiation. The scattering process takes place in the aforementioned virtual state-energy level of a vibrational or rotational level, and the energy change E of the photon demonstrates the difference between the elastic Rayleigh scattering and the inelastic Raman scattering. Also molecular rotational and vibrational frequencies can be determined directly, and from these frequencies it is sometimes possible to evaluate the molecular geometry, or at least to find the molecular symmetry. Even when a precise determination of structure is not possible, much can often be said about the arrangements in a molecule from empirical information about the characteristic Raman frequencies of groups of atoms.

The polymer samples investigations from this study involve the transition at a vibrational level. The scattering process at a vibrational level can be recorded with a change of the frequency ω or none. Rayleigh scattering represents the elastic scattering process since there is no frequency change ω and the energy E difference between the incident photon and the scattered photon is zero. Therefore transitions between energy level, initial state *i* and final

state f, will be considered to have $E_{fi} = E_f - E_i$, while the corresponding frequency is $\omega_{fi} = \omega_f - \omega_i$, meaning $E_{fi} = \hbar\omega_{fi}$. The other component of the scattering process shows the inelastic scattering of the photon which is described by the Raman effect. [96]

The change of frequency is described by the Raman scattering part- the Stokes and anti-Stokes scattering (differences shown in **Figure 2.6**). The Stokes Raman scattering refers to the transition from a ground vibrational state i and due to the absorption of energy the molecule will be promoted to a higher vibrational level f. The energy of the scattered photon is represented by the energy difference between the ground and excited level while the frequency of the light is red-shifted compared to the incident light. Due to the thermal energy molecules can be present also in a higher energy level. Thus, the anti-Stokes scattering concerns the inelastic scattering that occurs from a higher vibrational level f and reaching the final state on a lower vibrational level i. Here the light is blue-shifted while the energy of the scattered photon is represented by the energy difference between the ground and the excited level. At room temperature the population of molecules of an excited vibrational state is lower compared to the ground state according to Boltzmann's factor, which proves that the intensity of the Stokes scattering signal is higher than the one of the anti-Stokes process. In this case the signal of the anti-Stokes scattering will increase only when the temperature rises. [97]

In a schematic representation (see **Figure 2.6**) it can be distinguished between the Rayleigh scattering, which doesn't imply any energy exchange $\Delta E = 0$, and also between the Raman processes Stokes- with the energy variation $\Delta E = \hbar (\omega_0 - \omega_{fi})$ and anti-Stokes $\Delta E = \hbar (\omega_0 + \omega_{fi})$. [96, 97]
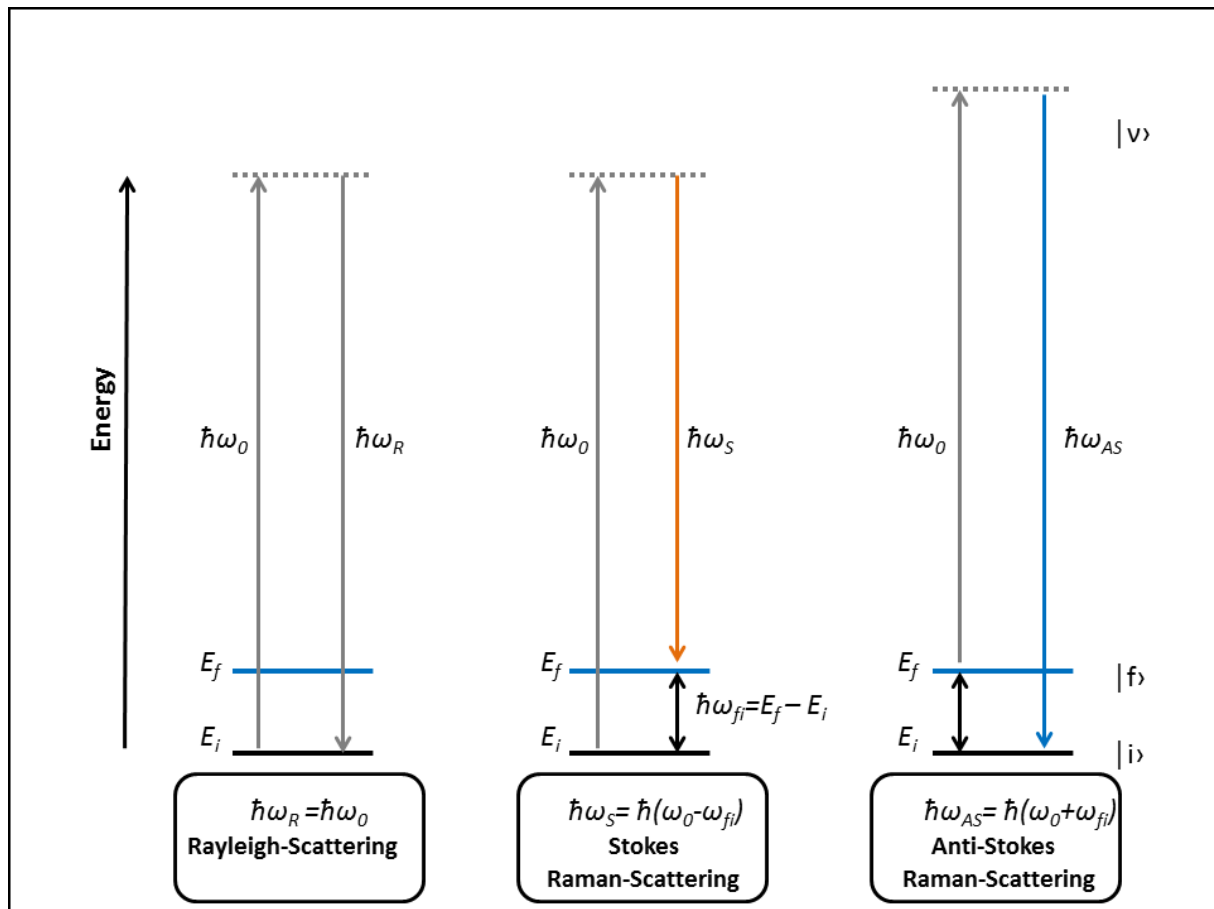
Figure 2.6 *Image presenting a schematic presentation of the Raman scattering (Stokes and Anti-Stokes scattering) and Rayleigh scattering.*

Even for the general investigations Raman spectroscopy is a non-invasive method, little or no sample preparation is required, and the samples can be easily handled. For instance **liquid samples** are placed in tube cells or in melting point capillary tubes, while of small amount of **powder samples** have to be placed on a holder or simply under a microscope that is part of the Raman micro-spectroscopy setup. Samples like **single crystals** can also be positioned on a normal microscope table. A sample that consists of **thin films** could behave similarly to a powder sample. In the next part some overall example of Raman analysis of different samples with different chemical structures, in different state of matter shall be presented.

A great number of possible analyses have presented themselves, when applying Raman spectroscopy in several different domains. Just as a reminder, one can enumerate successful studies in so many areas, i.e. in material science, biology (or sub-domains like biochemistry, biomedicine), pharmacy, mineralogy, or art. [98]

Characterization studies in the polymer research activity prove that qualitative investigations by means of Raman spectroscopy have been possible since their structure allows fast and facile Raman measurements. Compounds like polybutadiene [99], polyisoprene but also polyethylene [100, 101], or the degradation of vinyl polymers like poly (vinyl chloride), poly (vinyl bromide), poly (vinyl alcohol), or poly (vinyl acetate) [102, 103] were analyzed. Sulfur based polymers (mercaptans, polysulfides, or cyclic sulfur compounds) have been successfully characterized since the C-S and S-S bond provide a clear Raman scattering. [99, 104] One experimental approach to facilitate the spectral assignments is site-specific labeling of (macro)molecules, e.g. by deuteration. A plausible explanation for the overlapping bands in the C-H stretching region of the poly(methyl methacrylate) deuterated compounds investigated by means of Raman spectroscopy. The assigned vibrational modes were attributed to methylene, α-methyl and ester methyl groups of the polymer. [26] Thus, presenting the influence of the deuteration process, along with the expected changes of the molecular movements, example which will be found in the course of this study.

On the other hand the Raman spectroscopy can also offer well-grounded investigations on a quantitative level. This information can be extracted following the direct connection between the intensity of the Raman signal and the concentration of the investigated species, e.g. determining two different concentrations present in the same system. When the compounds are unknown then an internal standard is required, in order for Raman spectroscopy to be able to differentiate between two types. For instance in this case it is relatively facile to determine the composition of copolymers or as well of multi-constructed polymers. Here the data interpretation is based on the relative intensities of the Raman recorded data and the comparison of specific bands corresponding to characteristic components to the already established internal standards.

Having as a target the investigation concerning new types of chemistries, sometimes is difficult to have strict interpretations of the measurements just performed. To this extent a better assignment of Raman bands can certainly use the help of theoretical simulations. Therefore, the computational method DFT is the most employed strategy, which is a quantum mechanical modeling method that will exhibit an accurate presentation of the electronic structure of atoms and molecules. By comparing the theoretically generated spectra obtained with DFT calculation, to the recorded Raman spectra, reliable assignments will be possible and furthermore, a complex understanding of the electronic and geometrical structure of the investigated compounds will be available.

In the lines of this section a short overview of the Raman spectroscopy employment was presented. It was important to notice the sample types and structures that can investigated, the working-procedures when using a Raman setup. On the other hand, the most important aspect when characterizing several types of samples is to observe the specific "fingerprints" (characteristic features) obtained through Raman spectroscopy. Distinct vibrational modes were discovered, established and assigned for certain polymeric structures, pattern that was validly used in this study as well. This analytical method is ensuring the possibility of creating data bases able to provide complete vibrational modes assignments facilitating, for instance, the investigations of novel materials.

3. Experimental methods

In this section a complete description of the Raman microscopy setup will be given, method used in both the azide-alkyne cycloaddition and in the Diels-Alder reaction, followed by a short introduction into the setup responsible for the temperature treatment applied in the case of the crosslinking agents characterization. A following final part of this section will show the Density Functional Theory (DFT), method employed for the theoretical generation of Raman spectra in order to support the experimental recorded data. Although some of the methods were design to function for both cases of the investigated samples, there are a few differences that will be observed at the time of description. A brief presentation of the employed samples will be available in the end of this section.

3.1 Raman micro-spectroscopy setup

The spectroscopic instrumentation used in the experiment involving individual characterization of the main compounds that participate in the azide-alkyne cycloaddition, as well as the monitoring of the reaction while a temporal profile could be established is presented in the following lines.

Raman spectra were recorded using a micro-Raman setup (HR LabRam inverse system, Jobin Yvon Horiba) equipped with a frequency-doubled Nd/YAG laser at 532 nm with a laser power incident on the sample of about 4 mW. The laser beam was focused on the polymer sample using an Olympus 10x microscope objective. The dispersive spectrometer has an entrance slit of 100 μm and is equipped with a 300-grooves/mm^{-1} grating resulting in a spectral resolution of~ 1 cm^{-1}. The Raman scattered light was detected by a CCD camera operating at 220 K. The acquisition time per spectrum was 10 s. For calibration of the spectrometer, titanium dioxide (anatase) was measured repeatedly as a reference control for subsequent data processing.

For the spectroscopic Raman measurements performed for the individual characterization of the crosslinking agents (furan and maleimide), as well for the temperature treatment of the maleimide methacrylate samples, the above already described Raman setup was employed. The minor differences that occur in the experimental procedures in this particular case refer to the fact that the baseline correction and peak identification was based on the wavelet

transformation algorithm developed by Zhang et al. as implemented in R (script for background correction presented in Supplementary Information **S.1**). [105] For statistical treatment, the Raman bands were fitted with Lorentzian functions to calculate the peak area. Spectra smoothing was performed with Origin 8, Savitzky-Golay method [106] with a factor of 5.

3.2 LTS420 Linkam stage setup

In order to study if the chemical changes associated with the formation of reversible crosslinks (concerning the furan protected maleimide compound), and their temperature-induced opening and closing, result in changes, which can be detected by micro-Raman spectroscopy, a temperature-ramp Raman experiment is performed. During the individual temperature-runs the temperature of the sample was increased in increments of 10 °C every 10 minutes. This protocol provides a sufficient temporal window for spectroscopic monitoring of the sample and avoids artifacts from thermally non-equilibrated samples zones and minimizes any temperature fluctuations. Also, as one can observe in the below image (see **Figure 3.1**) installing and supervising the temperature-cell-stage under the microscope is a rather difficult task, which involves constant monitoring of the in-focus Raman measurements.

For the temperature-ramp experiments a heating system is used consisting of two hot-stages (here LTS420- see **Figure 3.1**), which are optimized for isothermal sample analysis applications.

Figure 3.1 *Experimental setup of the LTS420 heating/freezing stage, installed onto the*
Raman microscope setup.

For this instrumentation setup a compromise was made between the high-speed heating and cooling system, with a larger sample area and a thermal stability of less than 0.1 °C. The LTS420 is a heating/freezing stage operating in the temperature range between -196 and 420 °C, which consists of a large area temperature controlled element with a platinum resistor sensor embedded close to the surface for accurate temperature measurements. The sample is mounted on a standard microscope slide in direct contact with the heating element. The sample chamber is gas tight and has gas valves to purge the sample with either inert gas or an atmosphere with controlled humidity. [107]

3.3 Density Functional Theory (DFT) calculations

DFT calculations were performed using the Gaussian 09 program suite. [108]

In order to reduce computational cost only the molecular fragments necessary for the self-healing mechanism in the case of the azide-alkyne reaction the polymers were cut down to the structures necessary, while for the Diels-Alder cycloaddition this step involved the omitting

of the methacrylate structure from the calculations being aware that differences between measured and computed spectra might arise.

Structure optimizations were performed with the B3LYP [109-111], the long range corrected CAM-B3LYP [112] and the B3PW91 [109][113-115] hybrid functionals. Various basis sets were employed in order to find the best optimization method for the investigated molecules: The Pople basis sets 6-31G [116] and 6-311G [117][118] with and without the polarization functions by Frisch et al.as well as the diffuse functions by Clark et al. were tested. [119][120] Also the correlation consistent Dunning basis sets cc-pVDZ [121]and cc-pVTZ [122] with and without the diffuse functions by Kendall and Woon et al. were tested. [122][123]

The lowest energies were calculated with B3LYP/aug-cc-pVTZ in case of 2, 4, 2+4 and Alkyl. In case of PIB_NW and PIB_N3 not all calculations converged, therefore the best energies were obtained with B3LYP/6-311++g(d,p).

The lowest energies were calculated with B3LYP/aug-cc-pVTZ in case of 2, 4, 2+4 and Alkyl. In case of PIB_NW and PIB_N3 not all calculations converged, therefore the best energies were obtained with B3LYP/6-311++g(d,p), while the same combination of B3LYP and aug-cc-pVTZ was used in both cases, of furan and maleimide. Once the optimized geometries within the applied framework were identified, the respective molecular structures were used for calculating the Raman frequencies. To correct for the lack of anharmonicity and the approximate treatment of electron correlation, the harmonic frequencies obtained from the DFT calculations were scaled by factors that have been reported in the literature for similar systems. [124]

3.4 Materials

3.4.1 Poly(isobutylene) azide. Poly(isobutylene) alkyne

The investigated poly(isobutylene) samples consisted of self-healing polymers based on a poly(isobutylene) network. [19] Measurements were performed on the chemical compounds constituting this network (shown in **Figure 3.2**). This includes samples of the three-arm star poly(isobutylene) azide (PIB-$(N_3)_3$, M_n = 4,000 g/mol, M_w/M_n = 1.4) and a trivalent alkyne (M_n = 5,700 g/mol, M_w/M_n = 1.3).
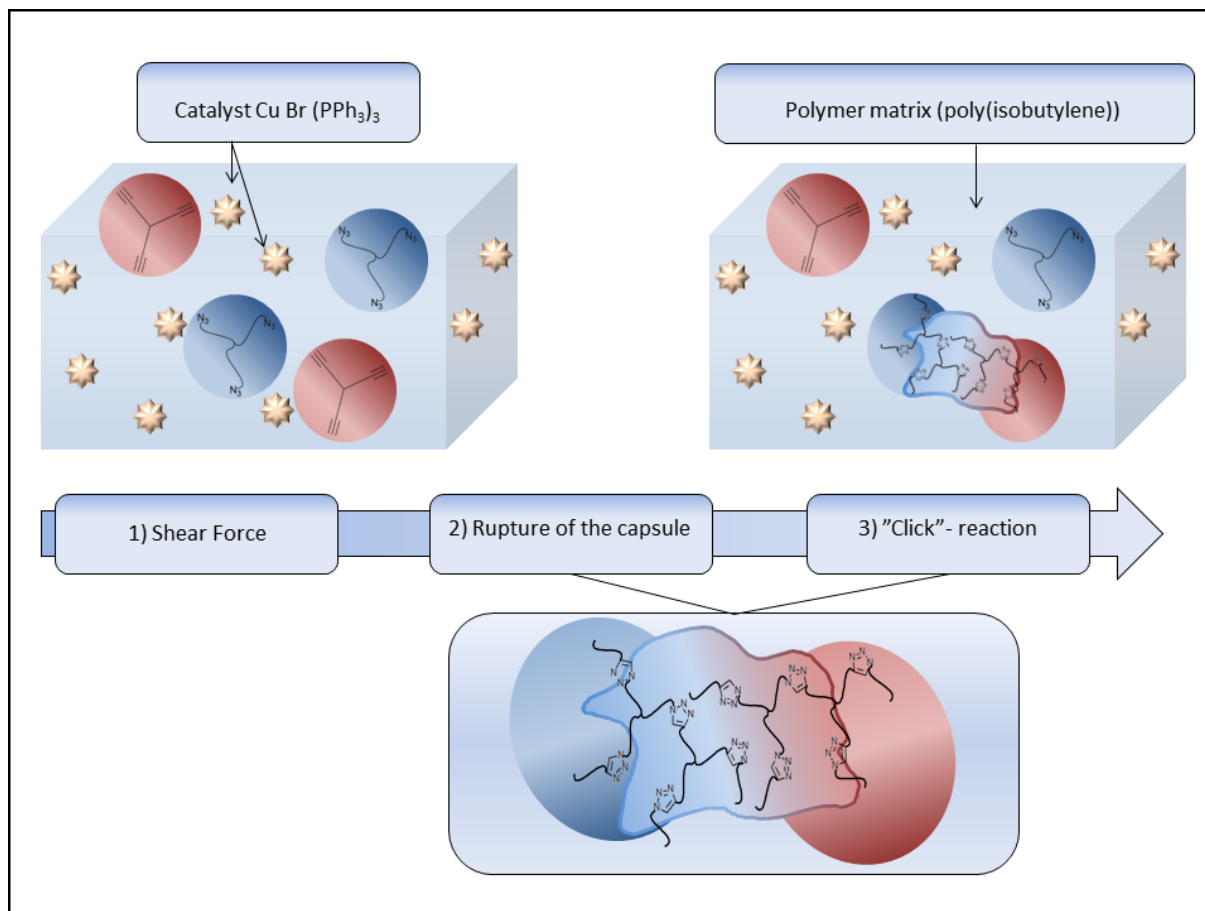
Figure 3.2 *Illustration of the general damage-behavior of the self-healing polymer coatings based on the pre-embedded microcapsules poly(isobutylene) matrix system, having as cornerstone for the self-healing mechanism the azide-alkyne copper(I)-catalyzed cycloaddition-reaction. The shear-force will break the polymer matrix, and the crack will rupture the microcapsules found on the damage trajectory, releasing the liquid healing agent into the polymer matrix. The reaction will take place once the healing agent will meet the present catalyst.* (adaptation to reference [82])

The scheme presented in **Figure 3.2** shows a demonstration of the self-healing process responsible for the repairment of polymer coating based on encapsulated microcapsules. Since the capsules can be randomly distributed in the polymer matrix structure, the polymer samples investigated in this work represent the complete polymer matrix that is formed after the capsules liquid burst out. Without the presence of the catalyst a complete analysis of the individual components can be noticed (presentation found in section **4.1**). Later on in this investigation, with the addition of the catalyst, a viable monitoring of the reaction (see **Figure 4.1** and **Figure 4.5**) can be established.

3.4.2 Furfuryl methacrylate. Maleimide methacrylate

The sample used in this study were synthesized by the cooperation partners J. Kötteritzsch et al. according to literature [16], i.e. the furan/maleimide units were covalently attached to a monomer. As previously described in the literature [125] the functional copolymers were synthesized with furfuryl methacrylate (FMA) and with an aliphatic bis(maleimide). Therefore, in this contribution furfuryl and maleimide with a methacrylate moiety were used as monomers for the Diels-Alder reaction (see structures in **Figure 4.8**). For a future overview concerning a complete application, this approach insures a complete functionalization, with no additional formation of second homo- or copolymer, species. In order to avoid crosslinking during polymerization, protecting groups for the furan or maleimide units are introduced. For that reason furan-blocked maleimide was used as a functional monomer. The thus obtained virgin polymer can be heated to initiate a retro-Diles-Alder reaction in the polymer side-chains. As a consequence the furan, which has initially protected the maleimide, evaporates and enables novel (reversible) crosslinks in the polymer matrix being formed upon cooling the material.

In this work the aim was directed toward Raman investigations of the methacrylate monomer-based samples, since this a precursor for the future formation of the polymer. The functional monomer used in this work was based on the successfully used approach [16] of a maleimide methacrylate compound, otherwise ascribed as furan-blocked maleimide monomer.

4. Results and discussions

This chapter presents the results obtained from the performed Raman measurements in the case of polymer-based azide-alkyne cycloaddition, as well in for the polymer sample based on the Diels-Alder reaction. Prior to any type of recorded data the focus of the investigations was directed to a detailed spectroscopic analysis of the individual components that were a part of the complete reactions. Once each chemical component, which is further involved with the reaction process, is analyzed and characterized, the proceedings for reaction monitoring can take place.

The first part of this chapter relates to spectroscopic investigations concerning the azide-alkyne cycloaddition, where detailed information will help the individual characterization the polymer-based samples of poly(isobutylene) azide and poly(isobutylene) alkyne, as well a short description of the Cu(I)-based catalyst. Afterwards, the next set of experiments worked toward a full monitoring of the azide-alkyne reaction with the main scope of establishing, not only a temporal profile, but also a clear understanding of chemical components behavior during the reaction. An important aspect of overall description will target the identification of specific Raman marker bands that could help demonstrating the initial expectations of this reaction.

The second part of this chapter will target the Raman investigations of the Diels-Alder reactions along with the separate characterizations of the incorporated crosslinking agents. As the already established trend, the first steps of the investigations will include individual spectroscopic analysis of the furfuryl methacrylate and the maleimide methacrylate components. A full observation of specific spectroscopic features of these chemical structures shall provide important information of the behavior at the room temperature (offering the possibility of determining characteristics Raman bands). To achieve a deeper insight into the behavior of these samples at higher temperatures, a separate experiment was developed involving the maleimide methacrylate component (which is a furan protected maleimide compound).

4.1 "Click"-reaction azide-alkyne [1]

Previously in this work several mentions (see subchapter **2.1.2 Types of self-healing mechanism**) have been made that the system responsible for the functionality of the self-healing mechanism involves the azide-alkyne "click" reaction. Multiple choices of investigation methods have demonstrated main features of the reaction itself and of the chemical components involved in the reaction. In the following lines a few examples of employed methods and the chemical derivatives will be discussed. The aim of this short presentation will focus on vibrational fingerprints characteristic for the chemical components investigated in this study. Also, specific wavenumber regions will be shown in order to create a clear pattern of the future analysis of the study at hand, presenting the Raman marker bands of choice.

Starting with general investigations of the CuAAC reaction, successful monitoring of the reaction was possible   using real time IR vibrational spectroscopy The authors Sun and Wu [127] identified the azido, alkynyl and 1,2,3- triazole reacting groups, following afterwards fingerprint regions which proved the use of the alkyne and azide during the formation of the 1,2,3- triazole product. Concerning the fingerprint region of the triazole clear identification was determined placing the region of interest at 900-1400 cm^{-1}. Another study based their monitoring of the azide-alkyne cycloaddition on the measurements performed with the help of IR spectroscopy (observing the loss of the azide band), NMR spectroscopy (the shifting of the methylene group in the direction of the azide group), or the behavior of the alkyne moieties analyzed by H NMR spectroscopy. [82] The complexity of this cycloaddition has been investigated following different strategies, using complementary investigation methods. Starting from a focused analysis of the reaction itself, it has later been observed that the reaction groups participating at the reaction need individual investigations.

Considering the fact that the alkyne Raman marker band in this study has been observed in a silent region, other studies have shown the same feature of the fingerprint region. Therefore, the authors Yamakoshi et al. [128] have performed Raman microscopy to investigated living cells containing alkyne-modified molecule, and they assigned the band found at 2123 cm^{-1} to

---

[1] The results presented in this section are published in:

 [126].   S. Vasiliu, B. Kampe, F. Theil, B. Dietzek, D. Dohler, P. Michael, W. H. Binder, and J. Popp. *Appl. Spectrosc.*, **2014**, **68**(5): p. 541-8.

the alkyne contribution. Similar bands have been registered for alkyne-modified oleic fragment using doubly-resonant four-wave mixing (DR-FWM) placing the characteristic alkyne stretching vibration at 2115 cm^{-1}. [129] Changes in the alkyne molecules have been also investigated by Stanghellini and Rossetti [130] while performing IR spectroscopy, mass spectrometry and elemental analysis on metal complexes. The structural modifications and the vibrational pattern of the alkynes signature were demonstrated with the changes of the frequency of the C≡C stretching mode (here registered at about 2142 cm^{-1}).

Azide components have also captured the attention of researchers, and investigations using several methods have demonstrated specific vibrational features. For instance FTIR [131] was used to analyze glycidyl azide polymer discovering small wavenumber shifts of the –CNNN skeleton when compared to the calculated data. Theoretical studies establishing the structure and stability of formyl azide CHO-NNN and methyl azide CH_3-NNN [132] , carbamoyl azide [133] or halosulfonyl azides [134] using DFT-B3LYP, have also brought a valuable support information concerning the azides vibrational modes assignments. In plus using FTIR and FT-Raman methods the carbamoyl azide has demonstrated a sharp peak at 2200 cm^{-1} assigned to the N≡N stretching.[135]

In-situ IR vibrational spectra was obtained for azide ions [136], while using IR and Raman spectroscopy (He-Ne laser) presented new aspects of the azide compound during the investigations of α-lead azide (PbN_6) [137]. In plus the same two aforementioned methods were used to analyze single crystal potassium azide [138], as well as IR investigations of the cyanogen azide [139]. Raman investigations of ammonium azide (NH_4N_3) [140] and silver azide [141] assigned the N_3 asymmetric stretch mode to the band found at 2079 cm^{-1}.

Early IR and Raman investigations of the triazole compound were inclined to assign the ring stretching mode to bands found in the wavenumber region 1380-1537 cm^{-1} [142], frequencies found also in the case of 3-mercapto-1,2,4- triazole using FT Raman and FT-IR [143]. Moreover the formation of the triazole compound has been recorded during the Cu(I)-Huisgen 1,3- dipolar cycloaddition, in which case Raman spectroscopy (as well as SERS) was performed on self-assembled monolayers of 1,4-diethynylbenzene on silver and gold. The triazole vibrational modes of interest were assigned to the bands found at 1348 cm^{-1} and 1533 cm^{-1}.[144] SERS together with DFT calculations has also demonstrated to be a good investigation method for the triazole ring stretching mode (bands found at 1425 cm^{-1} and 1447 cm^{-1}) found during the study of electrosorption of 1,2,3-triazole on gold. [145]

Since the main chemical compounds are already part of the polymer structure, the only necessary step is initiating the reaction, where in the presence of the Cu(I) catalyst the polymer network will present a new formed structure along with the occurrence of a triazole component. **Figure 4.1** summarizes the behavior of the reaction along with the chemical compounds used in this case, and as expected the development of the new formed poly(isobutylene) polymer branch.
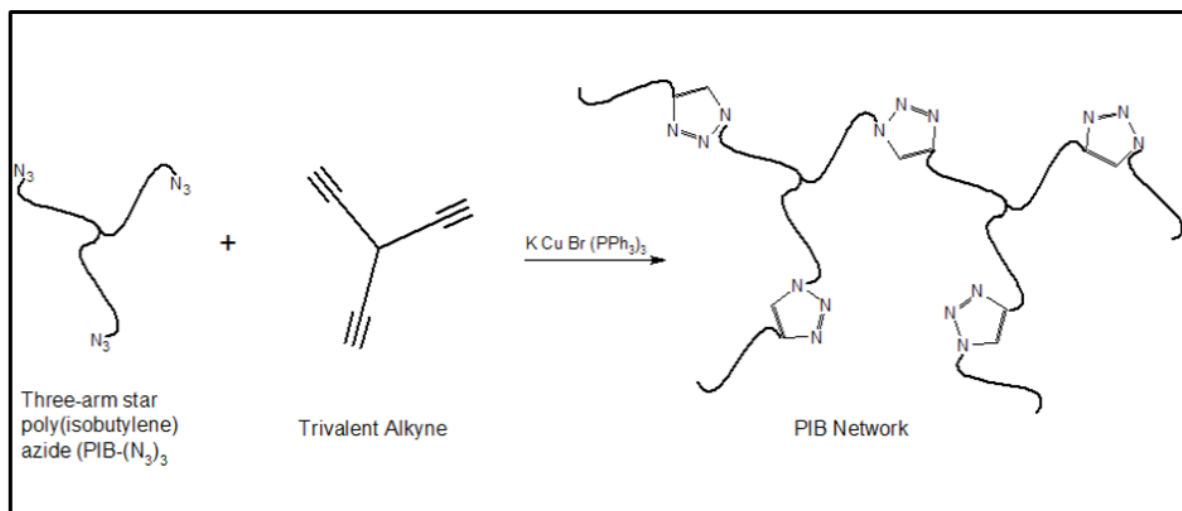
Figure 4.1 *Here is presented the azide-alkyne cycloaddition presents the poly(isobutylene) network formed upon the click-reaction between the three-arm star poly(isobutylene) azide (PIB-(N$_3$)$_3$), and the trivalent alkyne components.* (adaptation to reference [85])

During this study the experiments involved a detailed analysis and general observations have proved that, for a precise understanding of the fundamental reaction behavior, one must initially discover the particular spectroscopic characteristics of each reaction-involved chemical component. Thus in the next lines, as a primary step towards the investigations of polymer formation, distinctive investigations were performed for each particular chemical compound. As a short reminder it must be mentioned that the azide and alkyne components are analyzed in a more complex and complicated environment, since both of them are already attached to the poly(isobutylene) polymer matrix.

Due to the presence of the complex polymer system common features have been established for the recorded Raman data. Also, specific wavenumber ranges represented the subject of careful investigations, in order to establish specific vibrational modes as distinguishing "fingerprints" for each chemical component. To this manner, the experiments started with the individual characterizations of the poly(isobutylene) alkyne and continued with the

comparison of the analysis performed on the poly(isobutylene) azide. A short observation into the catalyst specific vibrational characteristics is available also, as a particular signature for the future investigations of the reaction profile.

4.1.1 Raman spectra of PIB Alkyne; PIB Azide; Cu Br (PPh$_3$)$_3$

Introducing the spectroscopic recorded data of the already mentioned alkyne-chemical component, **Figure 4.2** illustrates the general vibrational modes, where it can be easily noticed the preponderant influence determined by the poly(isobutylene) polymer presence. Nonetheless, the focus of the acquired data is shifted towards specific spectral signatures of the main chemical component- alkyne. Addressing this matter one can observe in **Figure 4.2** that the band was found at 2125 cm^{-1}, this aspect showing a particular importance since normally this wavenumber region is usually characterized as a Raman silent region. Therefore, the peak found at the aforementioned wavenumber can be assigned here to the -C≡C stretching vibration. [128, 129, 146]
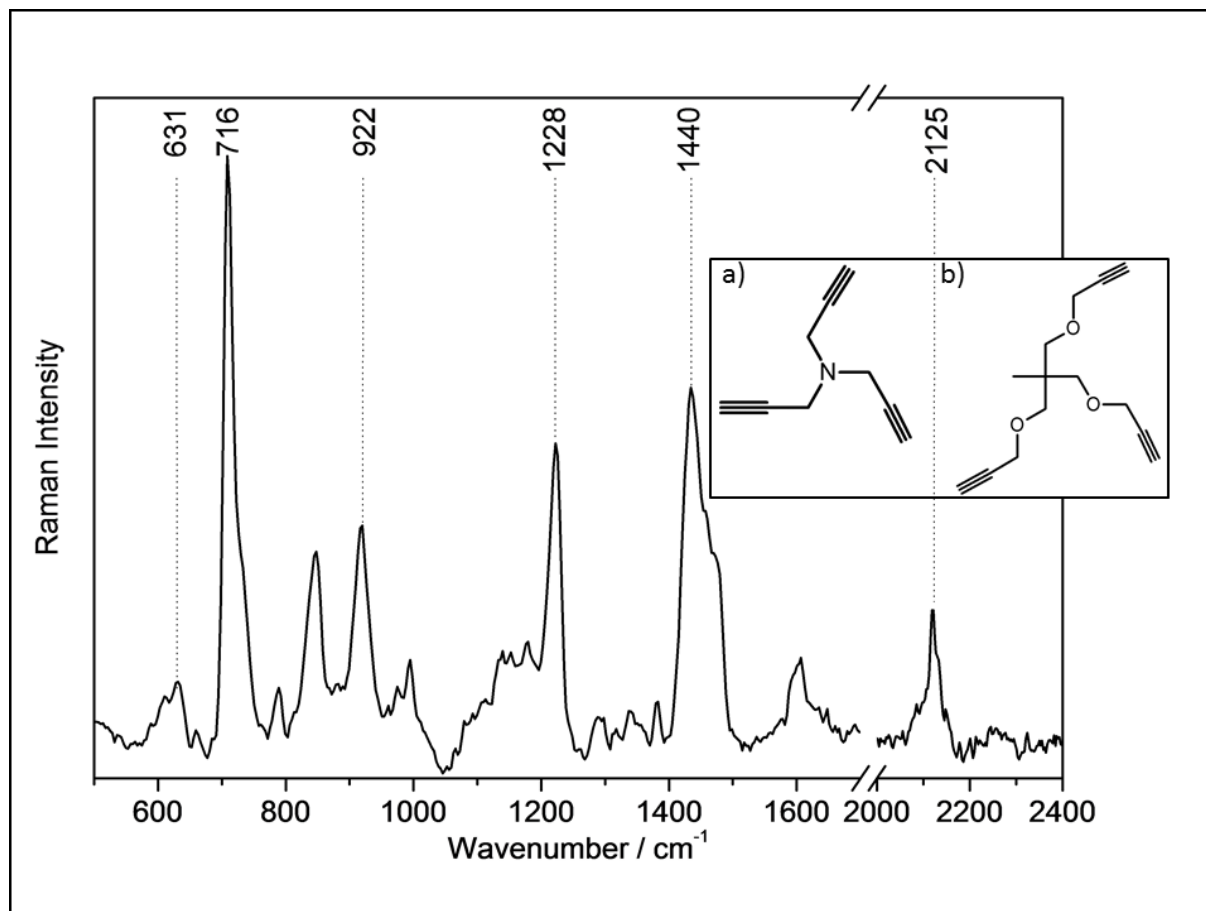
Figure 4.2 *This figure presents the experimental Raman spectrum of poly(isobutylene) alkyne. In the inset image on the right side the chemical structures of the low molecular weight alkyne are shown.*

This Raman band at 2125 cm^{-1} constitutes a valid marker band that can provide the necessary support for following the "click" reaction *in-situ*. The argument behind this choice is based on the fact that the assigned -C≡C moiety is converted during the reaction into the 1,2,3-1H-triazole component.

Distinguishing between the poly(isobutylene) polymer presence and the main components-azide and alkyne- the analysis of vibrational modes focused on presenting possible assignments of the predominant observed bands. Therefore, several different recorded bands will be discussed as it follows: the band found at 631 cm^{-1} was assigned to the C≡C-H bending vibrational mode, while the next strong feature found at 716 cm^{-1} is attributed to the C-H deformation mode; on the other side the lower intensity band recorded at 922 cm^{-1} can be explained with the stretching vibrational mode of the C-C≡C group and the next lower intensity band from 1228 cm^{-1} is a contribution of the CH wagging vibrational overtone

modes. Additionally one can observe the significant band at 1440 cm^{-1} is due to the C$_2$H$_3$N$_3$triazole ring.

The above analyzed figure (see **Figure 4.2**) presents important features of the targeted alkyne-component, but also follows closely specific vibrational modes of the polymer backbone. The obtained informations are of vital interest for the next part of the work since determining the behavior and spectral signatures of the poly(isobutylene) azide (shown in **Figure 4.3**) will present similar bands attributed to the polymer backbone. As a consequence, distinguishing characteristic features of the azide component should become a facilitated task.

Previously during this study an introduction of the theoretical calculations was presented, in order to support the experimental recorded data (which can create interpretation difficulties due to the complex information offered by the elaborate polymer structure). **Tabel 4.1** summarizes the theoretically generated wavenumbers while compared to the poly(isobutylene) alkyne experimental data. An appropriate and individual description of the assignments is also presented in the table.

Table 4.1 Experimental and theoretically calculated wavenumbers, and vibrational peak assignment of alkyne.

Wavenumber / cm^{-1}		Assignment
DFT	Experimental	
574	631	C≡C-H bending
698	716	C-H deformation
839	922	C-C≡C [a]stretch.
1283	1228	C-H wagging vibration overtone
	1440	C$_2$H$_3$N$_3$ ring [b]sym. [a]stretch.
2238	2125	C≡C [b]sym. [a]stretch.

[a]stretch=stretching; [b]sym=symmetric

As previously reminded the common structure of the poly(isobutylene) polymer backbone (also present in the azide samples) will influence and present similar spectral signatures also in the Raman recorded data of the next individually investigated sample of poly(isobutylene) azide. The complete spectrum is shown in **Figure 4.3**, where the most important observed bands are contained in a limited wavenumber region. One can notice that here there is no clear peak recorded in the ~ 2000 cm^{-1} wavenumber region.
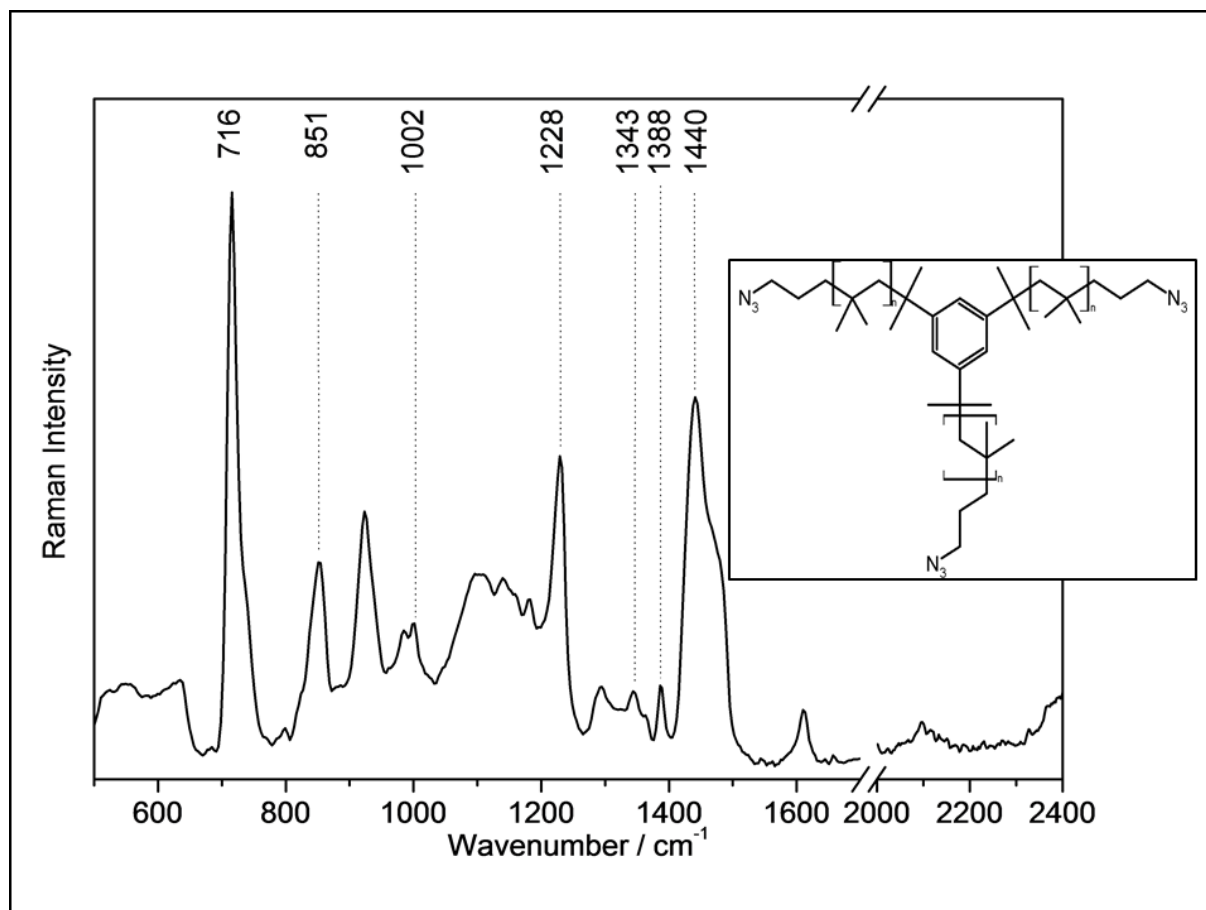
Figure 4.3 *This figure presents the experimental Raman spectrum of poly(isobutylene) azide, while in the inset image on the right side the chemical structure of the three-arm star azido-telechelic poly(isobutylene) is available.*

Although the polymer backbone has a strong influence in the Raman recorded data of the poly(isobutylene) azide sample (shown in the above **Figure 4.3**), there are a few features that can be discovered in the above spectrum. To this matter one can expect a more detailed illustration of peaks attributed to the triazole participant. In other words, several significant signals can be assigned like this: the sharp and high intensity band found at 716 cm^{-1} could be assigned to the torsion movement of the triazole ring, while the lower intensity signal

recorded at 851 cm^{-1} is interpreted to the CH wagging of the mentioned ring, and in the end, the band found at 1002 cm^{-1} is assigned to a ring bending mode of the triazole.

Next in line, other considerable bands can be found at 1228 cm^{-1}, which could be assigned to N$_3$ symmetric stretch of the azide group, while the next marked peaks found at 1343 cm^{-1} and at 1388 cm^{-1}, can be attributed to the symmetric stretching of the C-C, respectively to the wagging of the CH$_3$ group. Additionally a more accurate comparison between the theoretically generated wavenumbers and the experimentally recorded is available in the below table (see **Table 4.2**)

Table 4.2 Experimental and theoretically calculated wavenumbers, and vibrational peak assignment of azide.

Wavenumber / cm^{-1}		Assignment
DFT	Experimental	
674	716	C$_2$H$_3$N$_3$ ring torsion
845	851	C-H wagging of C$_2$H$_3$N$_3$ ring
941	1002	C$_2$H$_3$N$_3$ ring bending
	1228	C$_2$H$_3$N$_3$ ring [b]sym. [a]stretch.
	1343	C-C [b]sym. [a]stretch.
	1388	CH$_3$ group
1337	1440	C$_2$H$_3$N$_3$ ring [b]sym. [a]stretch.
2240		NNN [b]anti-sym. [a]stretch.

[a]stretch=stretching; [b]sym=symmetric.

A proper and complete observation is also required for the Cu(I) catalyst presence, since this chemical compound is also involved in the behavior of the "click" reaction. Some of the most significant bands will be discussed in the next lines. The Raman recorded spectrum solely observed for the Cu Br $(PPh_3)_3$ catalyst is presented in **Figure 4.4**.
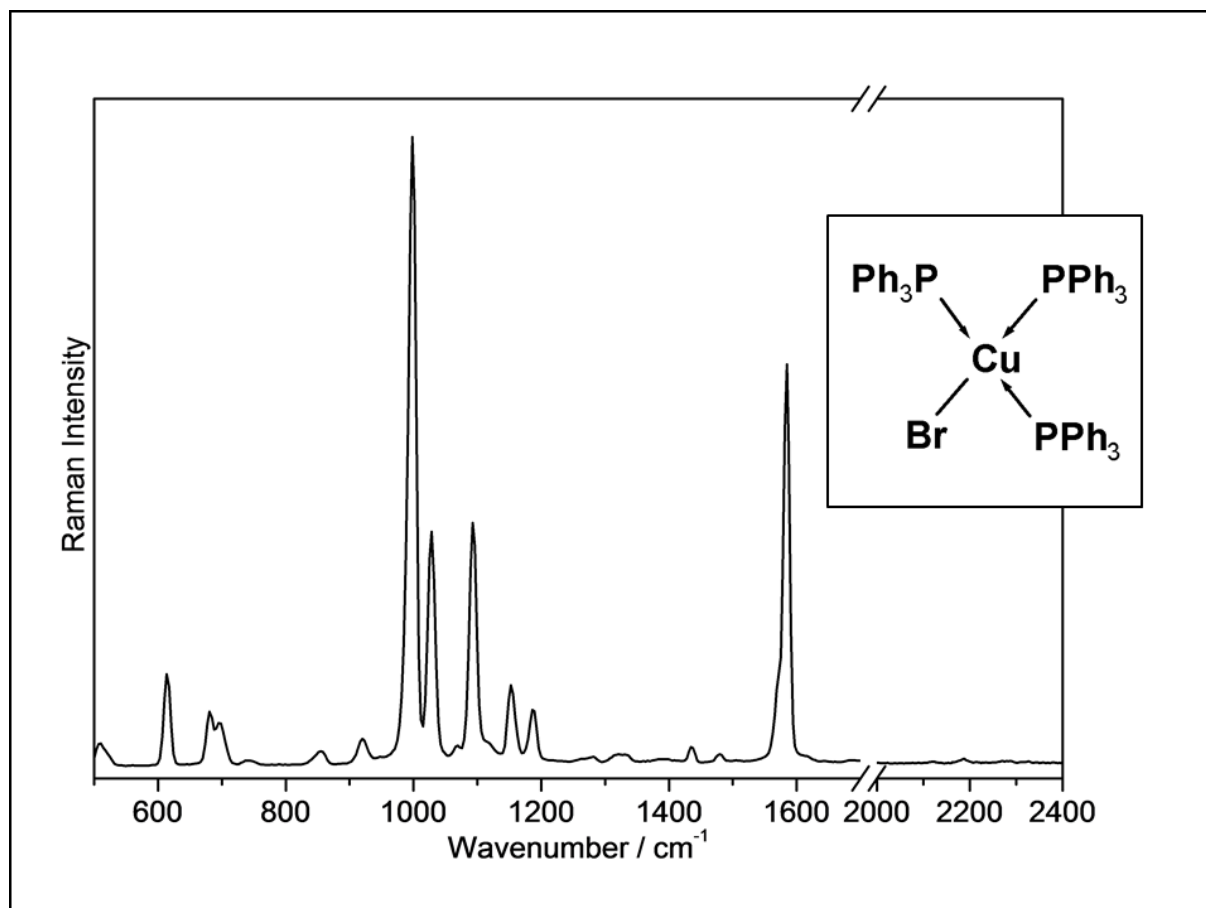
Figure 4.4 *Image showing the experimental Raman recorded spectrum of catalyst Cu Br (PPh$_3$)$_3$.*

The bands more accurately identified were found in the lower wavenumber regions, and they are assigned in the following lines: 508 cm^{-1} (phenyl *y* mode), corresponding in other studies to the band at about 445 cm^{-1} and at 512 cm^{-1}; the registered band at 612 cm^{-1} (phenyl *s* mode) found in literature [147] at bands 617 cm^{-1}, or 618 cm^{-1}; the peak observed at 681 cm^{-1} (phenyl *r* mode) presented in literature as attributed to wavenumbers found at 689 cm^{-1}, 695 cm^{-1}, or 708 cm . The band found at 857 cm^{-1}, although is in close vicinity to the mainly phenyl modes assignments, describes a high probability of a PIB mode, i.e., CH wagging mode. In fact, according to the literature [147, 148], most of the observed bands describing

the molecular behavior of the catalyst can only be assigned to the triphenylphosphine ligand of the catalyst.

4.1.2 Temporal profile of the azide-alkyne cycloaddition

Taking into account the presented data as a support for the PIB alkyne (see **Figure 4.2**) and PIB azide (see **Figure 4.3**) characterization, one can distinguish valuable information necessary to explain also the triazole presence within the PIB network. Thus, when a clear differentiation can be made, the recorded Raman band found at 1440 cm^{-1} is attributed to the symmetric stretching of the triazole ring, assumption which is in good correlation with theoretically reproduced data in the DFT calculations (compared data in **Tabel 4.1** and **4.2**), where the band is found at 1337 cm^{-1}. [145]

Since specific vibrational modes can be assigned and clear spectroscopic features of the main reaction participants can be identified, then other Raman marker bands can be defined offering a good end-point of the "click" reaction. With respect to this matter, it must be reminded that one of the Raman marker bands (the band found at 2125 cm^{-1}) has been already analyzed and considered to clearly monitor the changes that occur during the reaction.

To this regard, a separate experiment of this study focused on the *in-situ* Raman measurements which are shown in **Figure 4.5**. More in detail, monitoring the intensity behavior of the band at 2125 cm^{-1}, vibration assigned to the symmetrical stretching of the C≡C, will help with the construction of a reaction temporal profile. In plus, a great contribution to behavior of the reaction can be attributed to the new formed ring of triazole ($C_2H_3N_3$), which demonstrates the presence of expected features of the ongoing reaction.
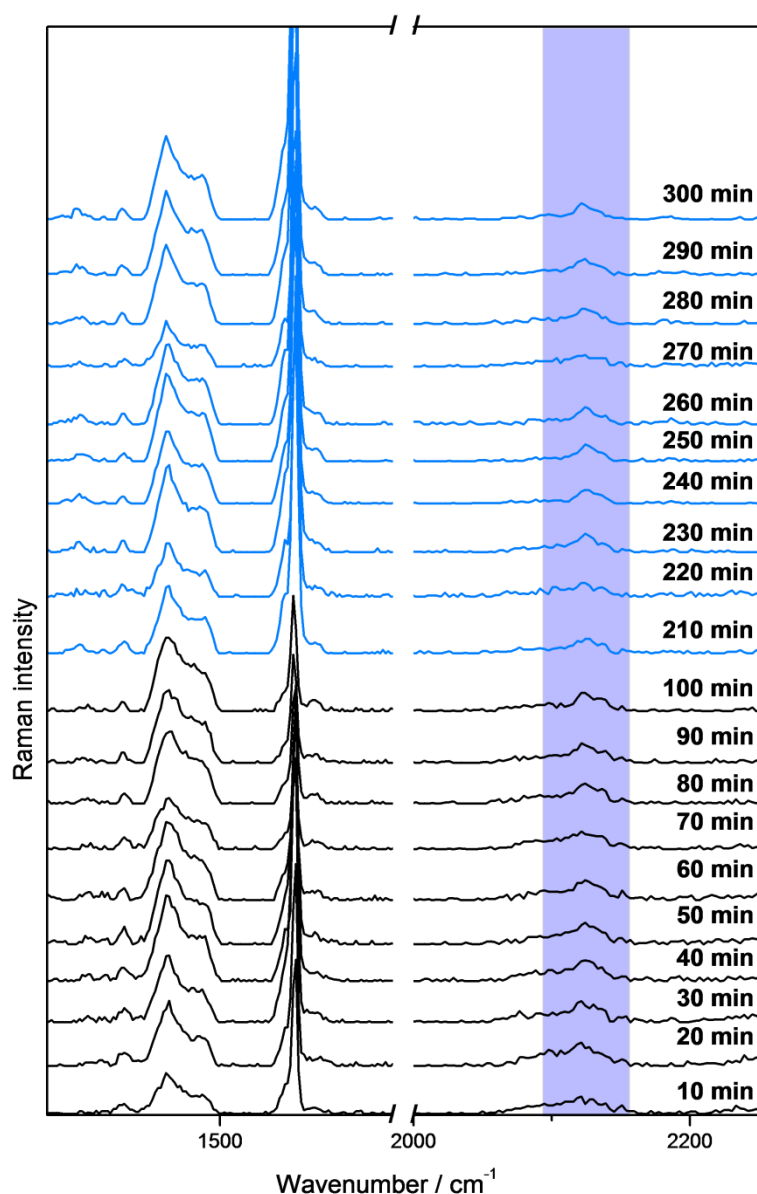
Figure 4.5 *In-situ measurements performed at 532 nm on poly(isobutylene) network along with the azide and alkyne component, and the catalyst. The reaction was followed for 300 minutes. Due to the fact that the reaction needs time to develop certain observable features, a Raman spectrum was recorded every 10 minutes, in order to observe changes in the Raman spectra during the course of the self-healing reaction (all measurements performed at room temperature).*

Data normalization was performed as primary step towards establishing the aforementioned temporal profile of the "click" reaction, based on the presented data from **Figure 4.5**. Therefore, in **Figure 4.6** one can find an elaborate description of the method used for spectra

normalization. A particular point of view must be taken into account: the normalization procedure is here specially needed due to the fact that there are no bands which could be used as external standards. To remove the signal fluctuations effect, Multiplicative Scatter Correction (MSC) was used. This spectra normalization method can be defined as follows: once a reference spectrum has been found the alignment of the intensity values is possible. In this case a mean spectrum serves as reference. [149]
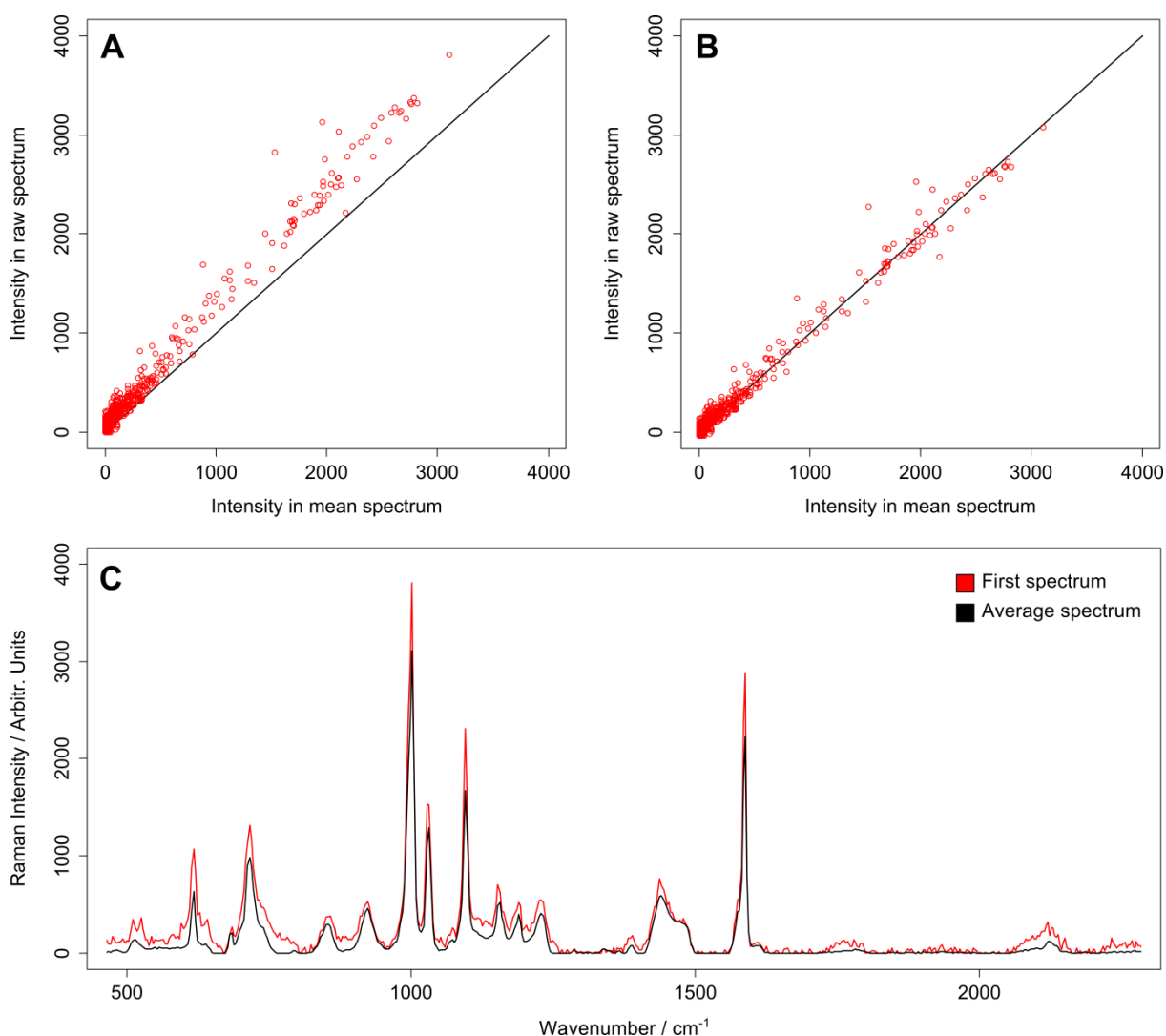
Figure 4.6 *Illustration of the MSC normalization describing the components used for finding the factor (mean spectrum before the treatment). Panel A presents the intensity values of the first spectrum, plotted against the corresponding values in the average spectrum. It can be seen, that the intensities of the first spectrum are consistently higher than the reference values. The algorithm evens out these differences by using regression to find a factor and a constant to map the raw values as closely as possible to the reference. In panel B it is shown*

that the majority of intensity values are centred on the marked black 1:1 ratio line after the

treatment with MSC. The image from panel C shows the spectra before treatment.

The previously mentioned spectra signal treatment will provide in the next part of this discussion, important information regarding the behaviour of the alkyne's triple bond feature, while monitoring the intensity changes of the band observed at 2125 cm^{-1}. Thus, the data analysis concerning this precise Raman band of the C≡C can be found in **Figure 4.7**.

Based on literature research [85], the statement that the reaction would provide a clear acceleration along the process founds to be valid. At the same time proving that certain compounds (as presented with the help of the band at 2125 cm^{-1}, describing alkyne's marker band) are used, while the presence of other new compounds (triazole) is clearly recorded during the reaction's process.

The graph shown in **Figure 4.7** presents analysis occurred after normalization procedure was executed. The Raman intensity at 2125 cm^{-1} found in the graph, describes the profile of the "click" reaction, all the information with respect to the time needed for completion.
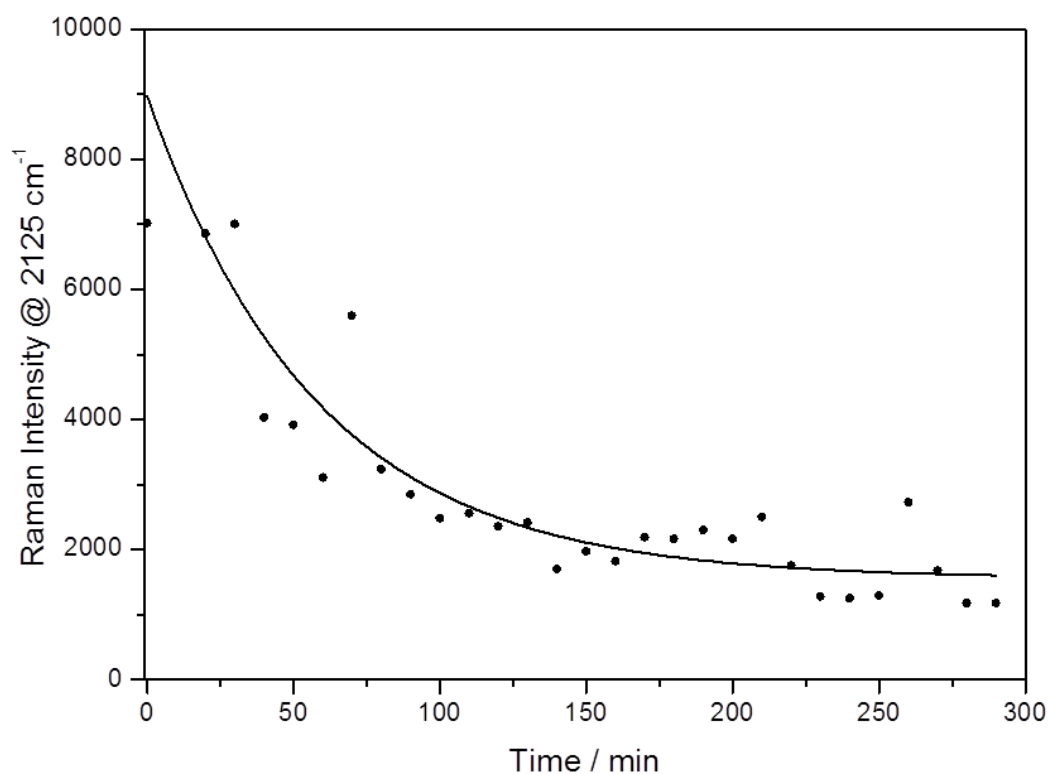
Figure 4.7 *This figure represents the behavior of the intensity at 2125 cm^{-1}, which is decreasing in time. The temporal profile shown refers to the azide alkyne click reaction*

underlying the self-healing in the polymer coating at hand. Dots indicate the original data, while full line represents an approximate trajectory of the decreasing intensity.

Following the information offered by the data processing from the graph shown in **Figure 4.7**, it can be stated that with the help of Raman spectroscopy, a quantitative description of the intensity behavior of the alkyne's vibrational mode (set here as maker band) is completely possible. As the graph presents the intensity of this band is decreasing in time, which demonstrates that the used alkyne compound in this reaction will facilitate the occurrence of the new-formed triazole. This hypothesis was presented within the "click" chemistry cycloaddition introduction.

From a technical point of view the necessary mention refers to the fact that, Raman measurements were performed on a single point on the investigated sample, therefore no other interference could disturb the chemical compound ratio, which is constant. This proves that the alkyne component disappears in time, as the graph in **Figure 4.7** shows with the decay curve of the intensity.

In this case, building a reaction kinetics profile of the reaction along with a quantitative presentation of the reaction becomes a difficult task to achieve. Probable links between the Raman band intensity of the alkyne band and a specific chemical compound concentration could demonstrate new features of the temporal profile.

In fact, the main scope of this full analysis was to provide a detailed view of the behavior of significant Raman bands. As a result of this study, obtaining information that could lead to the self-healing polymer coating characterization, while monitoring the azide-alkyne "click" chemistry.

4.2 Diels-Alder cycloaddition

As already presented, the Diels-Alder reaction, i.e. in general the cycloaddition of a conjugated diene and an alkene forming a cyclohexene system [150], of furan and maleimide has been employed in the design of self-healing polymer materials. In this context, studies on the impact of various polymer backbones on the DA reaction within polymer side-chains and the influence of various combinations of the self-healing units, maleimide and furan, have been performed. [151-153] As the basis for a micro-Raman investigation of the self-healing

polymers in this study, the state-of-the-art of vibrational Raman and IR-absorption spectroscopy on the molecular structures relevant for this self-healing study is summarized in the following: Furan itself has been studied by both Raman and IR vibrational spectroscopy [154], including its deuterated derivatives (furan-2-5-d_2, furan-3-4-d_2, and furan-d_4) [155], furan in the liquid (as a function of temperature and pressure) [156] and gas phase [157], as well as furan derivatives such as furfuryl alcohol- FA, furfural, hydroxymethylfurfural-HMF, and levulinic acid. [158] Infrared spectroscopy, on the other hand, was employed to study maleimide and isotopically labeled maleimide in the gas phase [159, 160] and maleic anhydride as well as the interaction maleimide with nitrogen, water and hydrogen chloride. [161] Information on the low-wavenumber modes, i.e. the vibrational and torsional motion of the methyl group and the maleimide ring are obtained from FT-Raman and inelastic neutron scattering. [162] Additionally maleimide was investigated using surface-enhanced Raman scattering (SERS), FT-Raman spectroscopy and DFT calculations. [163] Raman spectroscopic investigations of complex (macro)molecular are often complicated by overlapping vibrational bands and hence a complicated assignment of observed bands to distinct (macro)molecular vibrations. [164]

The work at hand provides the spectroscopic basis for subsequent microspectroscopic experiments on polymer films by demonstrating the potential of Raman scattering to resolve the specific chemistry of the temperature-dependent Diels-Alder and retro-Diels-Alder reactions within a polymer matrix. In this work it will be presented that the sensitivity of Raman-scattering by itself and in combination with site-specific deuteration of the side-chain groups in methacrylate polymers, bearing furan and maleimide units in the side-chains, is sufficient to employ this method as a tool to study the polymer formation, which is a forerunner for the self-healing processes in polymer samples.

The next section of this work includes a more detailed characterization of the polymer formation, and in this context, polymers that will behave under the non-autonomous self-healing mechanism features (see **Figure 2.5**). As already mentioned in the work at hand, the non-autonomous intrinsic self-healing mechanism is the cornerstone for materials that need an external trigger, in order to function as a self-healing system. In this particular case the self-healing mechanism will be initiated by applying a higher temperature. The intrinsic character of this type of mechanism proves the existence of a build-in self-healing system that will only need to be activated. At the same time the possibility of several cycles of system healing represents another advantage. In intrinsic self-healing reversibly switchable bonds are

integrated into the functional network. [165] Upon an external trigger such as heat [48] or absorption of UV light [47] the reversible bonds open, structural rearrangement of the matrix can take place and finally the reversible bonds are reformed, thus restoring the material properties.

It has to be evaluated if the sensitivity of Raman spectroscopy is sufficient to detect the chemical changes associated with the wide-chain reactions on the background of the spectroscopic response of the polymer host matrix. In this contribution the question is addressed specifically focusing on the self-healing polymers, in which the **reversible bonds,** which are indispensable for autonomous self-healing of the material, are provided by (retro) Diels-Alder-reaction of furan and maleimide units.

4.2.1 Furfuryl methacrylate and maleimide methacrylate

The chemical structures studied in this work are summarized in **Figure 4.8**. The furan and the maleimide unit, respectively, are covalently attached to a methacrylate monomer, which – after polymerization – will yield the polymer backbone of the self-healing coating. In this study, the focus will turn to the spectroscopic characterization of the respective monomers and the retro-Diels-Alder reaction of the protected maleimide-methacrylate. DFT calculations were performed in order to assign the experimentally observed Raman bands, which were recorded for both the furan (furfuryl methacrylate FMA) and the maleimide (maleimide methacrylate) moiety (for structures and compared spectra see **Figure 4.8**, respectively **Figure 4.9** and **4.10**).
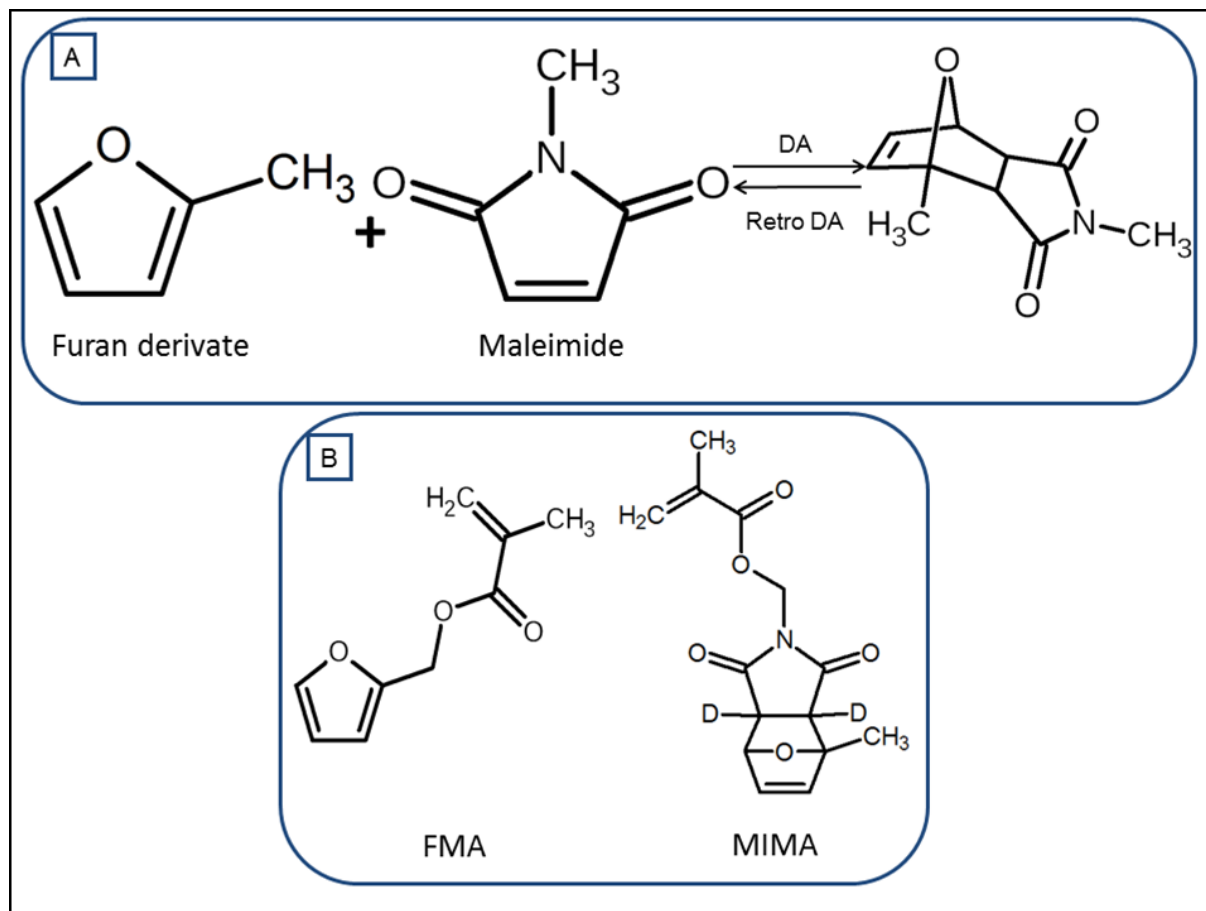
Figure 4.8 *Schematic representation of the self-healing concept via reversible DA reactions as well the chemical structures of the crosslinking agents furan and maleimide (panel A presents the structures simulated by the DFT calculations), and the structures of the analyzed samples furfuryl methacrylate- FMA, and maleimide methacrylate- MIMA (shown in panel B, where the figure illustrates the deuterated compound).*

Outlining the basic Raman spectroscopic characterization of the of the crosslinking agents, in the next lines a detailed presentation will be available. The first investigated case was concerning the furan based sample, and as shown in **Figure 4.9** experimental recorded data is compared to the theoretically generated spectra. Since the investigated MIMA compound represents the joined presence of furan together with the maleimide component, the spectra comparison involved a different approach from the furan characterization. Here, the recorded Raman spectra of MIMA (see **Figure 4.10C**), was compared with the theoretically generated spectra of maleimide (shown in **Figure 4.10A**) and the component of furan together with maleimide (shown in **Figure 4.10B**).
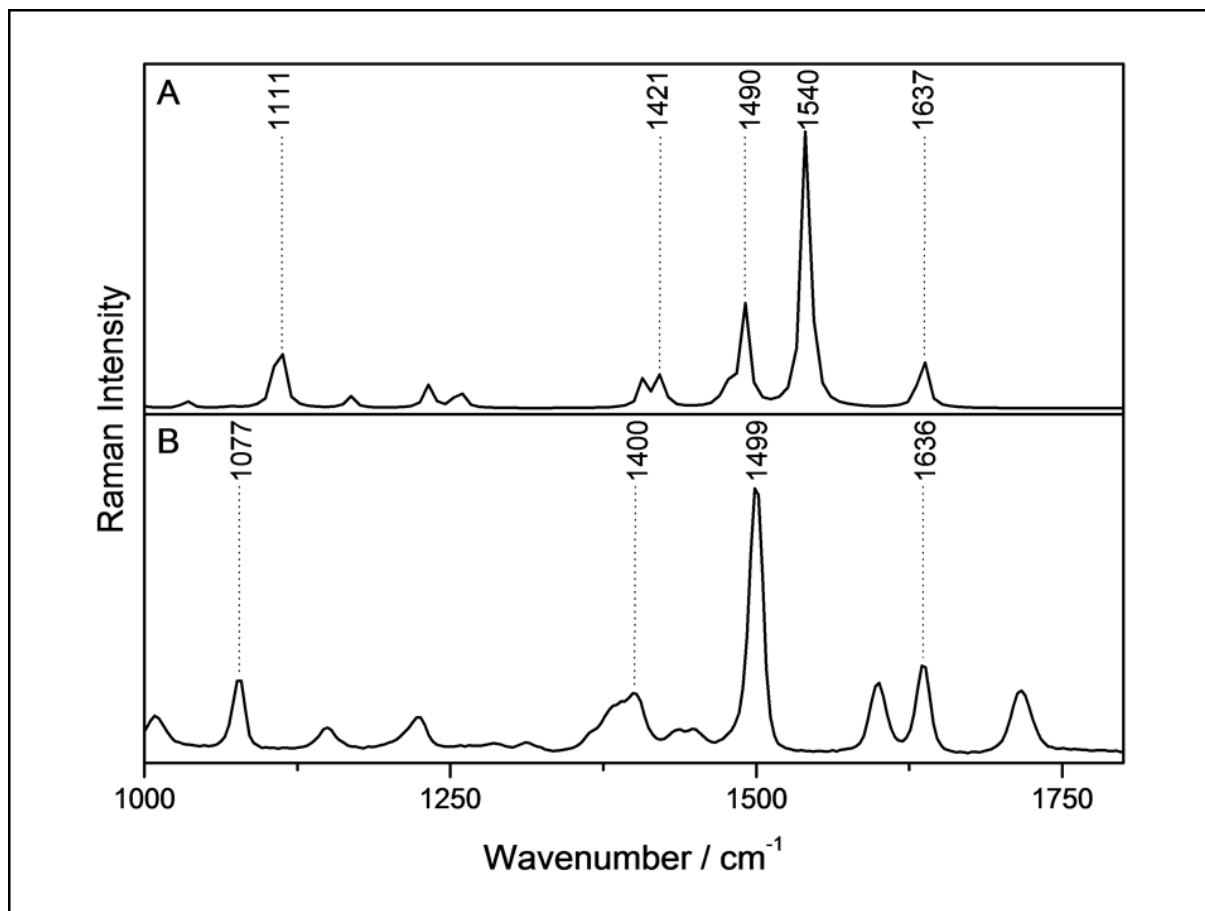
Figure 4.9 *The panels of this image display the calculated Raman spectrum of furan (panel A) and the experimental spectrum of furfuryl methacrylate- FMA (see panel B), respectively, upon excitation at 532 nm.*

Figure 4.9 compares the experimental Raman spectrum of the relevant furan-methacrylate monomer (recorded at room temperature) with the theoretically derived spectrum: The spectra of furan are dominated by bands between 1000 and 1800 cm^{-1}. The Raman active vibration at 1077 cm^{-1} (1111 cm^{-1} in the calculated spectrum) is due to C-O stretching. The deviation in band position between the calculated and the experimental spectrum is assigned to the fact that the DFT calculations were performed for isolated furan, while the experimental data was for the furfuryl methacrylate (FMA), which presents the monomeric unit for the macromolecular synthesis of the self-healing polymers. [16] Another intense Raman active mode of furfuryl methacrylate is observed at 1400 cm^{-1}. This mode is assigned to C-C stretching based on the DFT calculations, which predict the center of the band to appear at 1421 cm^{-1}. Generally the vibrations in the region of 1600 cm^{-1} are assigned to C=C stretching vibrations. [155] [158] Finally, the band at 1636 cm^{-1} coincides well with the prediction of a C=C stretching vibration at 1637 cm^{-1} by DFT.
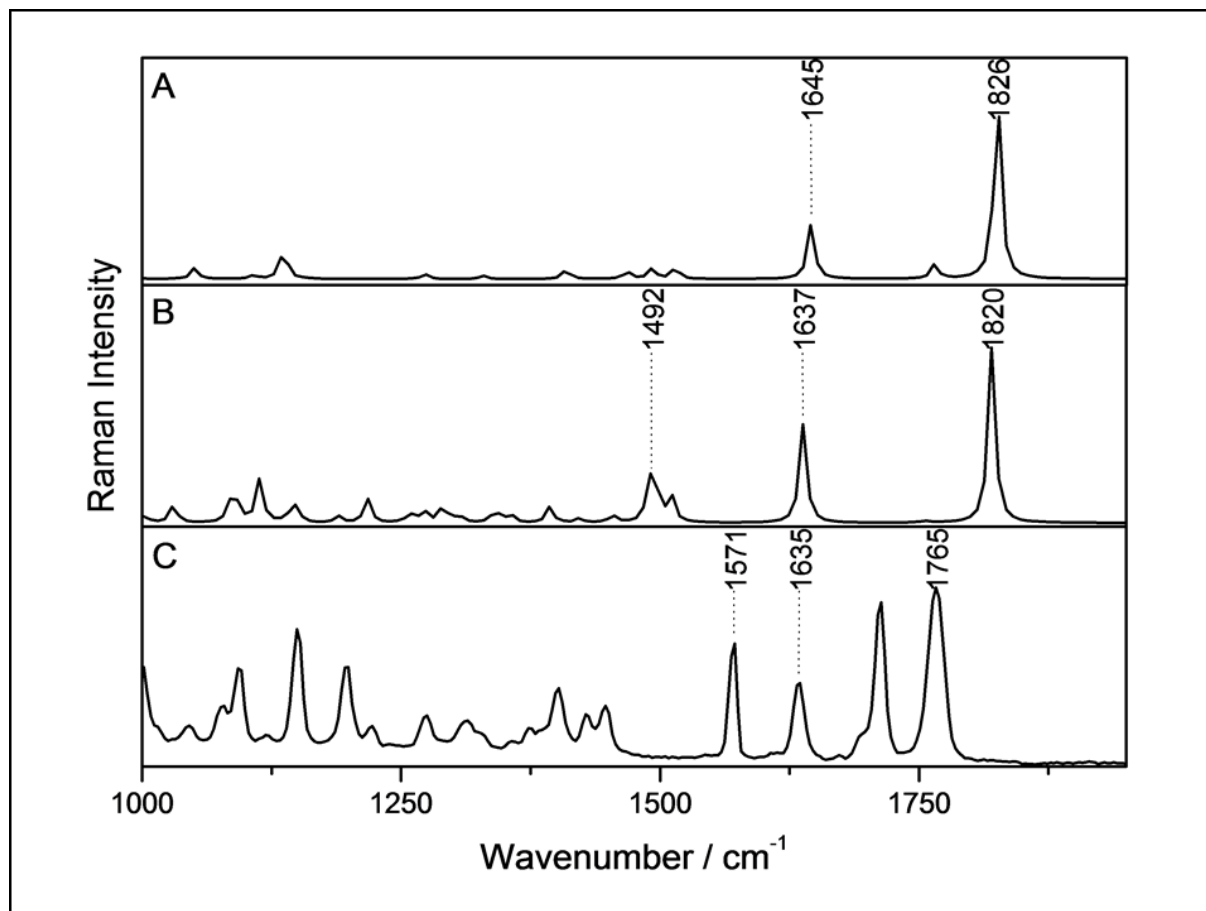
Figure 4.10 *The image shows the theoretically derived spectra of maleimide (panel C) and the product of maleimide together with furan (panel D) are compared to the experimental Raman spectra of maleimide methacrylate- MIMA (excitation wavelength 532 nm - panel E).*

The main task of the spectra comparison shown in **Figure 4.10A-C** is to accordingly assign the fundamental vibrational modes. For instance, at 1492 cm^{-1} C=C bond vibrations are observed, which should be characteristic for the individual components taking place in the reversible crosslinking reaction.

If the cycloaddition takes place as expected then the respective spectral region might be suited to follow the course of the temperature-induced retro-Diels-Alder reaction, in the course of which furan should evaporate from the sample, as previously stated in the literature [16]. This chemical change is expected to occur in concert with a loss of intensity of the Raman bands at 1492 cm^{-1} as can be judged from the calculated spectra shown in **Figure 4.10A** and **B**. In contrast, the vibrational modes observed at about 1640 cm^{-1} are rather invariant when comparing the data shown in **Figure 4.10A-C**. This can be understood when considering the presence of the C-C bond of the maleimide in either of the investigated structures. This

vibrational mode is furthermore not ideal to investigate the anticipated Diels-Alder-chemistry in the self-healing polymers as the maleimide vibration overlaps with the Raman active band at 1636 cm^{-1} in the experimental spectrum of furfuryl methacylates. Next, the C=O stretching vibration of the maleimide is observed at around 1800 cm^{-1}. **Figure 4.10A** shows the calculated spectrum of maleimide with a peak at 1826 cm^{-1}, while the calculated Raman spectrum of the DA product of furan and maleimide reveals a mode at 1820 cm^{-1} (**Figure 4.10B**). These bands could represent suitable marker bands to distinguish spectral contributions from maleimide and furan (furfuryl metacrylates) as the Raman spectrum of the latter does not show any bands above 1740 cm^{-1}. However, it should be noted that the calculated and experimental Raman spectra of the maleimide compounds differ significantly: The experimental spectrum (**Figure 4.10C**) – in contrast to the calculated ones (**Figure 4.10A** and **B**) does not reveal any bands above 1800 cm^{-1}. The ascribed shiftings (1714 cm^{-1}, 1765 cm^{-1} respectively) are attributed to the presence of the methacrylate monomer.

4.2.2 Maleimide methacrylate - temperature treatment experiment

The targeted scope of the previous analysis, as well as the description of the vibrational behavior, was intended to follow the Diels-Alder cycloaddition and the two crosslinking agents. The obvious initial premise was to distinguish between the characteristic features of the furan and maleimide compounds, in relationship to the investigated samples furfuryl methacrylate and maleimide methacrylate.

On this matter, having discussed the Raman spectra of the individual crosslinking agents and the DA reaction product of maleimide and furan in some detail, the focus of the investigations is shifting now to studying the furan-blocked maleimide methacrylate by temperature-ramp Raman spectroscopy. Thereby, spectroscopic insights into the course of the reaction underlying the possible exhibited performance of the Diels-Alder cycloaddition in the respective methacrylate-materials can be derived. Compared set of spectra are presented in **Figure 4.11** with panel **A** showing the recorded data of MIMA compound, while panel **B** of the figure presents the Raman recorded data of the deuterated species.
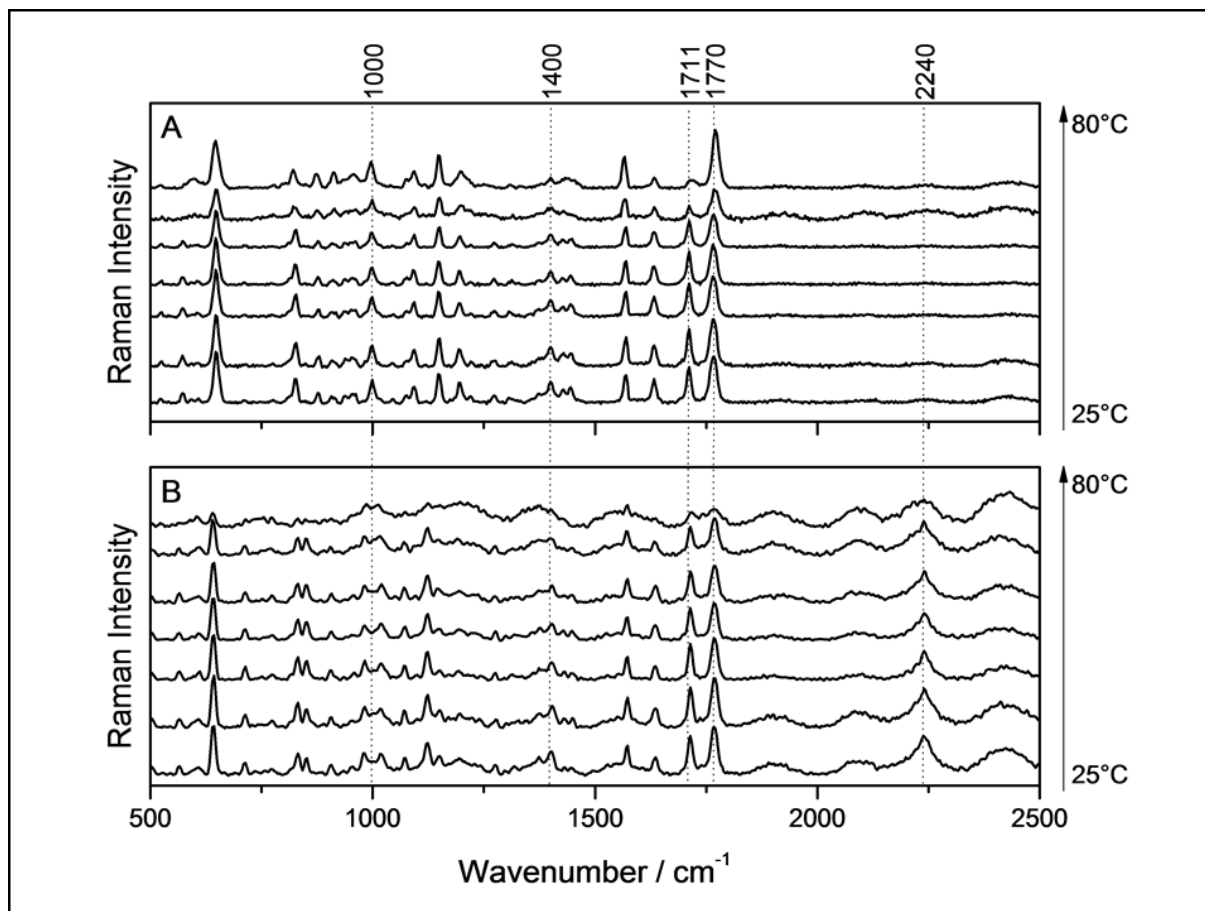
Figure 4.11 *Experimental Raman recorded spectra of furan blocked maleimide moiety (panel A) compared to the deuterated furan blocked maleimide system (panel B). Vibrational behavior observed during temperature treatment.*

During the temperature-ramp experiments the temperature of the sample was increased from 25 to 85 °C in increments of 10 °C every 10 minutes followed by acquisition of Raman spectrum at each temperature. Each spectrum displayed in **Figure 4.11A** and **B** represents a mean spectrum of three individual experimental spectra. **Figure 4.11A** displays the Raman spectra of the furan-protected maleimide methacrylate sample at increasing temperatures, thus the spectra reflect the chemical changes, which are expected to happen during the first cycle of the self-healing polymer coatings, which are based on the polymerized building blocks characterized in this study (see **Figure 4.8**). As mentioned above, in the virgin samples the furan units are "blocked" by the maleimide compound. The vibrational behavior observed in the recorded Raman spectra (presented in both panels of **Figure 4.11**), shows important marker bands (fundamental vibrational modes) that will could serve to future clarifications of the Diels-Alder reaction response. Additionally the experimental spectra (recorded during temperature treatment, presented in **Figure 4.11**) are found to be in a good agreement with the

calculated spectra (shown in **Figure 4.9** and **4.10**), this way a reliable characterization of the furan blocked maleimide methacrylate monomer being presented.

To increase the sensitivity of Raman spectroscopy in probing selective molecular fragments, selective deuteration of molecular structures has proven great potential. [166, 167] Following this general strategy, maleimide methacrylate-MIMA was selectively deuterated in the positions indicated in **Figure 4.8B**. The effect of the deuteration on the Raman spectra of the compound is shown in **Figure 4.11B**. Most prominently the CD-stretch vibration appears at 2240 cm^{-1}. Furthermore, deuteration causes significant shifts of the bands at 1016 cm^{-1}, 1403 cm^{-1} and 1714 cm^{-1} (shown in **panel B** of the **Figure 4.11**), which are associated with the normal modes of the non-deuterated sample at 1000 cm^{-1}, 1400 cm^{-1} and 1711 cm^{-1} (shown in **panel A** of **Figure 4.11**). Nonetheless, the overall Raman-active mode pattern of maleimide methacrylate in the fingerprint region remains qualitatively unchanged upon deuteration (shown by the 1770 cm^{-1} bond). For both the non-deuterated and the deuterated species temperature-ramp experiments are conducted to evaluate if the spectroscopic changes upon reversible bond-opening and –closing are detectable on the background of the polymer matrix.
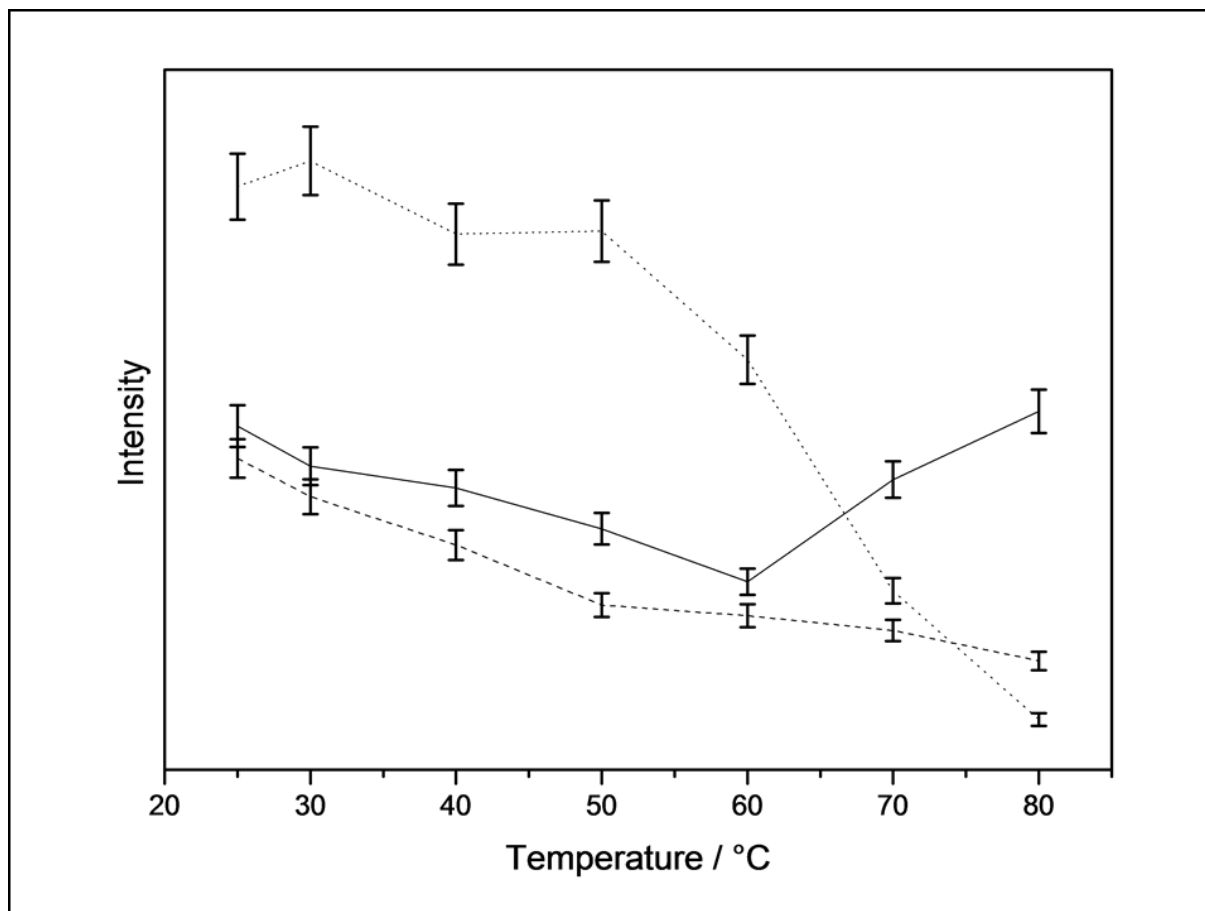
Figure 4.12 *Figure shows the temperature-dependence of selected vibrational modes belonging to the furan blocked maleimide moiety (panel A) (@ 1000 cm^{-1}- solid line, @1400 cm^{-1}- dashed line, @1711 cm^{-1}- dotted line, see panel C) of interest, following the same procedure while performing the temperature treatment.*

To illustrate the temperature-dependent changes in the Raman spectra of the self-healing polymer associated with opening and closing reversible molecular linker units, **Figure 4.12** comprises the temperature-dependent intensities of selected Raman bands. Raman spectra were recorded for temperatures up to 80 °C (where the melting point for furan is found at -86.5 °C, while for maleimide is at in the range of 91-93 °C) as upon further increase of the temperature fringe-artifacts are detected, which are likely to be attributed to scattering from the melting sample. To illustrate the overall temperature-dependent behavior of the Raman spectra the discussion is focused on the bands at 1400, 1711 and 1000 cm^{-1}.

In addition to the 1400 cm^{-1} vibration (representing the furan C-C stretching) the Raman active mode at 1711 cm^{-1} (assigned to the methacrylate C=C stretching) shows a characteristic temperature-dependent behavior: the integrated band intensity decreases with increasing

temperature, which can be directly related to the evaporation of furan from the sample as a result of the retro-Diels-Alder-reaction (in the case of the vibrational mode found at 1400 cm^{-1}). As for the case of the mode found at 1711 cm^{-1}, the explanation comes from the additional participation of the behavior of the monomer during the polymerization process. The course of this reaction should in principle be also reflected in the characteristic vibrations of the maleimide. To this end the discussion is focused on the 1000-cm^{-1} band, which is due to the asymmetric C-N-C in-plane bending vibration. [163] However, following the furan-evaporation hypothesis, the experimental data shown in **Figure 4.12** cannot straightforwardly be understood: The intensity of the 1000 cm^{-1} mode initially decreases but – at temperatures higher than 60 °C – increases again. Lower intensities were expected as a result of the increased temperature, and of course was expected as well the vibrational modes assigned to furan will show a low intensity. The latter band-intensity increase is unexpected based on the assumption that the evaporation of furan causes the initial drop of the band upon elevation of the temperature. Converging this discussion on the behavior of the sudden intensity increase of maleimide vibrational mode, is has been discovered that the high temperature treatment can interfere with the normal expectations of the furan blocked maleimide compound. Therefore a possible explanation for this effect might be stem from the autopolymerization. Controlled autopolymerization of styrene-N-butylmaleimide has been observed at elevated temperatures. This autopolymerization can take place when radicals are generated by thermal dissociation. [168] This interpretation is in line with a Raman-spectroscopic study on the polymerization of styrene and methacrylate, which reported a band at 1631 cm^{-1}, corresponding to the C=C stretching vibration of the polymerizable groups, to be a sensitive spectroscopic marker for the progress of the polymerization. [169] A qualitatively identical behavior is observed in the data shown in **Figure 4.11**: The band at 1711 cm^{-1}, which is assigned to the C=C stretching vibration of the methacrylate unit (see above), decreases slowly upon increasing temperature – both for the deuterated and the non-deuterated system. Hence, this finding corroborates that autopolymerization takes place during our temperature-ramp experiments and contributes to the spectroscopic characteristics observed here.

During this study the present investigations were able to prove a different approach for the characterization of primary stages of the retro-Diels-Alder cycloaddition between furfuryl methacrylate and maleimide methacrylate, in a temperature-ramp *in-situ* Raman study. For a better understanding of the underlying molecular changes, and a future employment of the crosslinking agents for the self-healing mechanism, Raman marker bands were established,

and furthermore a detailed description of these fundamental vibrational modes was presented. Additionally, unexpected behaviors were found to be present, for instance the noticeable influence of the autopolymerization, which offered the appropriate interpretation for the sudden change of intensity band pattern.
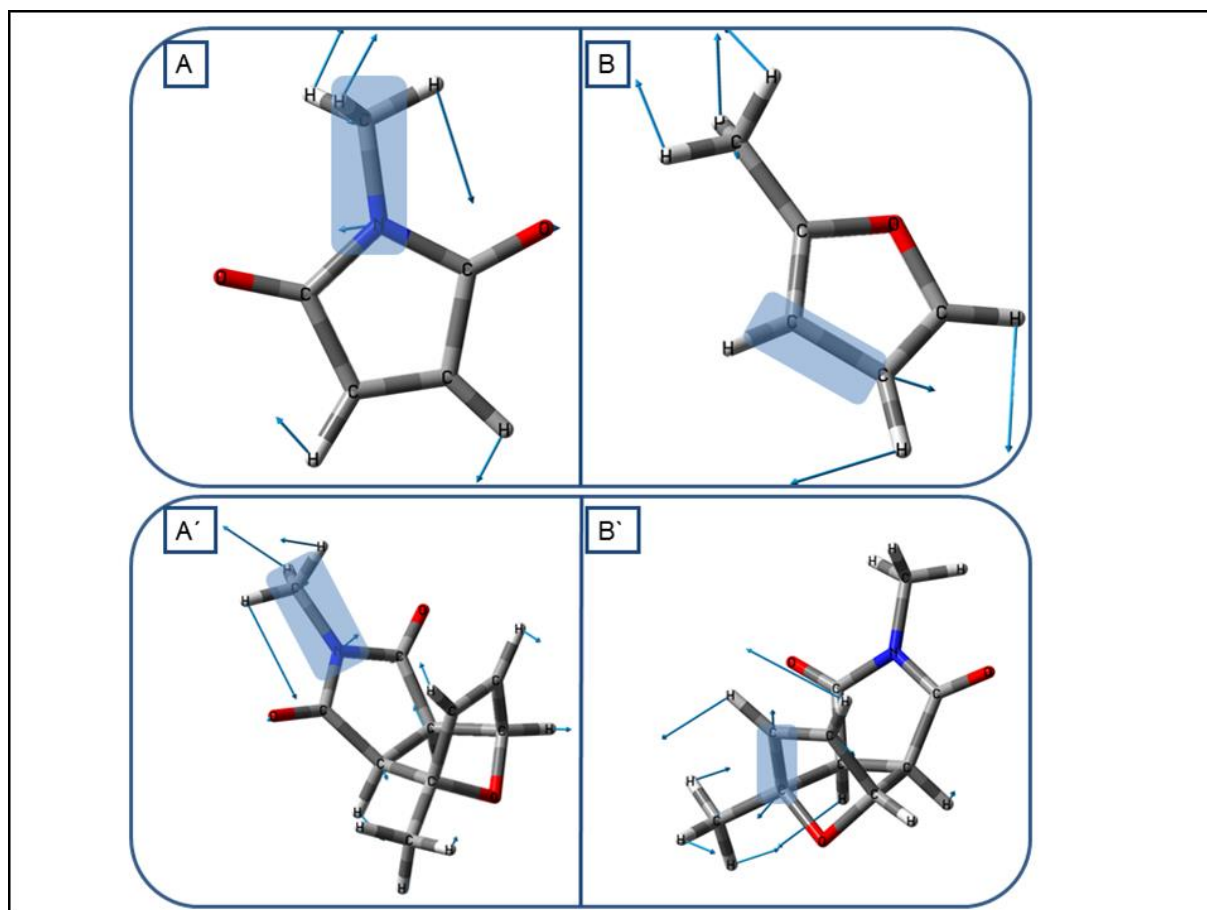
Figure 4.13 *Vector plots of the characteristic vibrational modes previously presented in this work. The bonds are presented in the calculated structures (density functional theory calculations). The panels A`, B` present the theoretically generated structure of the product between furan and maleimide. This way panel A and A` represent the vibrational mode found at 1000 cm$^{-1}$ (A- shows the theoretically generated structure of maleimide); in panel B and B` the vector plots corresponding to the bond found at 1400 cm^{-1} (panel B shows the theoretical calculations of the structure of furan). In the maleimide methacrylate compound the vibrational band was found at 1000 cm^{-1}, while in the panel A (theoretically generated maleimide) one can notice the band at 949 cm^{-1}, respectively in panel A` (theoretically generated product structure) the wavenumber is shifted to 980 cm^{-1}. (Here the assignment*

was performed according to the density functional theory calculations where the methyl stretching could engage a movement of the C-N-C). Also the vibrational mode found at 1400 cm^{-1}, is present in panel B (theoretically generated furan structure) at 1408 cm^{-1}, respectively at 1355 cm^{-1} in panel B` (theoretically generated product structure). Here the vector plots indicate a C-C stretching mode.

5. Conclusions

Self-healing polymer coatings are a subdomain of the new smart materials which possess a build-in ability of repairing the damage of the primary structure. The present study reports on Raman spectroscopic investigations characterizing the polymer formation. Monitoring the reaction behavior has also validated a set of first steps on the analysis of the molecular structures. Moreover this study shows another approach for performing investigations, one that was able to expand the understanding of the self-healing mechanisms from a different perspective, from an angle that is more detailed oriented and one that could explain the chemical changes underlying microscopical insights of the processes.

In the first part of the chapter Results and Discussions, the analysis of the self-healing polymer coatings based on azide-alkyne cycloaddition [19] revealed an important contribution of Raman characterization of the analyzed self-healing polymer coating, together with apprehension of the involved mechanism.

The measured spectra compared with theoretical calculations made possible the assignment of marker bands for the alkyne, azide and triazole. In the measured Raman spectra the polymer matrix poly(isobutylene) was showing a much stronger signal than the chemical components of interest (alkyne, azide, trizole). Differentiating between the Raman marker band region of the azide and alkyne was another task that led to the characterization of the vibrational mode of the triazole formation [142]. With all this said, it must now be reminded that the next step consequently leads this contribution to the temporal profile of the azide-alkyne reaction itself.

This analysis creates a closer overview of the chemical reaction by closely following their behavior in relationship to the full polymer system. Supervising and analyzing this mechanism in a linear connection with the chemical behavior of the reaction, can prove to be a valid analytical path for such self-healing polymer coatings.

This way Raman spectroscopy has proved to be a successful tool to monitor the changes that occur during this reaction. Therefore, the characterization of the reaction course could form an initial step for the description of the autonomous self-healing mechanism, showing as well the changes that are characteristics to the assigned molecular vibrations. [126] To sum up on the first part of the experimentally obtained results, Raman spectroscopy proved to be an

advantageous method due to the non-invasive character, therefore not influencing the normal course of the reaction rate.

On the other hand in the second part of the chapter Results and Discussions, during this work an insight into the analysis on self-healing polymer coatings based on Diel-Alder cycloaddition has been presented.[16] This new approach explains a complete and improved new starting point for further experiments on this kind of self-healing materials. This means that during this study the focus was directed to the elucidation of the cardinal points of the chemical reaction that is developed and also to perform experiments and measurements that will individually characterize the present chemical components.

As mentioned, a complex characterization of the involvement of the two main crosslinking agents, maleimide and furan, was possible. The predetermined marker bands identified as fundamental modes demonstrate the polymer formation along with explaining the reaction flow during the high-temperature treatment. Relative concentration of the reaction agents have been monitored by analyzing the intensities of Raman marker bands.

The results of this work present a well-grounded starting point for the investigations of the formation of the polymer coatings with self-repair features. Having the advantage of presenting the underlying molecular behaviors, the spectroscopic analysis from this work can offer significant and beneficial information for future evaluations of self-healing polymer coatings.

Deutsche Zusammenfassung

Selbstheilende Polymerbeschichtungen gehören zu den sogenannten „Smarten Materialien" und besitzen die intrisische Eigenschaft Beschädigungen, an ihrer primären Struktur, selbst heilen zu können. Die vorliegende Arbeit beschäftigt sich mit der Raman-spektroskopischen Charakterisierung der Polymerbildung. Durch die Beobachtung des Reaktionsverhaltens konnten die ersten, nötigen Schritte zur Analyse der molekularen Strukturen validiert werden. Darüber hinaus verfolgt die vorliegende Studie einen Ansatz, der sich auf das detaillierte Verständnis der chemischen Prozesse konzentriert, die den mikroskopischen Prozessen zu Grunde liegen.

Im ersten Teil des Kapitels „Results and Discussion" werden die Raman-spektroskopische Charakterisierung eines selbstheilenden Polymers, basierend einer Azid-Alkin-Cycloaddition, beschrieben und wichtige Erkenntnisse zum Mechanismus abgeleitet.

In den gemessenen Spektren konnten mit Hilfe theoretischer Berechnungen Markerbanden für Alkin, Azid und Triazol identifiziert werden. Trotz der deutlich stärkeren Ramansignale der Polyisobutylen- Polymermatrix konnten die chemisch relevanten Komponenten unterschieden und somit die Triazolbildung charakterisiert werden. Dies führte konsequenterweise zur Untersuchung der Zeitabhängigkeit der Azid-Alkin-Reaktion.

Durch diese Analyse wird ein tiefergehendes Verständnis der Bildungsreaktion in Beziehung zum gesamten Polymersystem erhalten.   Das Verfolgen und Analysieren des Reaktionsmechanismus stellt einen valide analytischen Weg zur Untersuchung von selbstheilenden Polymeren da.

Die Raman-Spektroskopie erwies sich dabei als geeignetes Werkzeug um die Veränderungen während der Reaktion zu verfolgen. Die Charakterisierung des Reaktionsverlaufs anhand von charakteristischen Schwingungsbanden ist dabei ein erster Schritt zur Beschreibung des autonomen Selbstheilungsmechanismus. Die Raman-Spektroskopie erweist sich dabei als eine wertvolle nicht-invasive Methode.

Im zweiten Teil des Kapitels „Results and Discussion" wurden selbstheilende Polymere auf der Basis der Diels-Alder-Cycloaddition untersucht. Diese Arbeit stellt einen neuen und verbesserten Ansatz für weitere Untersuchungen zu selbstheilenden Materialien dar. Der Fokus der Untersuchungen lag auf der Bestimmung von Kernparametern der chemischen

Reaktion, um Experimente zur individuellen Charakterisierung der chemischen Komponenten durchführen zu können.

Dadurch wurde die Charakterisierung der verbindenden Hauptkomponenten, Maleinimid und Furan, möglich. Die identifizierten Markerbanden erlaubten die Beobachtung der Polymerbildung und die Aufklärung des Reaktionsverlaufs während der Hochtemperaturbehandlung. Die Analyse der Ramanmarkerbandenintensitäten erlaubte die Bestimmung von relativen Konzentrationen der Reaktionsteilnehmer.

Die in dieser Arbeit präsentierten Ergebnisse setzen eine solide Grundlage zur Untersuchung der Bildung von selbstheilenden Polymeren. Die Untersuchung des zugrundeliegenden molekularen Verhaltens, durch spektroskopische Analyse, bietet signifikante und wertvolle Einsichten für die zukünftige Evaluierung selbstheilender Polymere.

S.1 Attachments (R script for background correction)

```
bgr_stat<- function(pattern="txt",lambda, SNR, wn1, wn2)

{

    library(baselineWavelet)

    addToFn<- "_bgRm"

    # get all files with respective pattern

    files<- dir(pattern=pattern)

    peakAreaList<- list()

    peakArea<- c()

    peakPos<- c()

    # for each file do processing as follows

    for(i in 1:length(files))

    {

            # read file

            Spektrum<- read.table(files[i]

            # get indices of defined wavenumber region

            if(wn1 <= wn2)

    {

            index<- which((Spektrum[,1] >= wn1) & (Spektrum[,1] <= wn2))

    }else{

            index<- which((Spektrum[,1] >= wn2) & (Spektrum[,1] <= wn1))

    }

    limits<- range(index)

            # get wavelengths (xa) and counts (x)

    x=Spektrum[limits[2]:limits[1],2]

    xa=Spektrum[limits[2]:limits[1],1]

            # set parameters

            scales<-seq(1, 30, 1)

            wCoefs<- cwt(x, scales=scales, wavelet='mexh')
```

```r
# plot

image(1:nrow(wCoefs), scales, wCoefs, col=terrain.colors(256), axes=FALSE, xlab='index', ylab='CWT coefficient scale', main='CWT coefficients')

box()


# get maxima = peaks

localMax<- getLocalMaximumCWT(wCoefs)

ridgeList<- getRidge(localMax, gapTh=3, skip=2)

plotRidgeList(ridgeList)

# peak identification

majorPeakInfo      =      identifyMajorPeaks(x,      ridgeList,      wCoefs, SNR.Th=SNR,ridgeLength=5)

# get peak width (at the baseline)

peakWidth=widthEstimationCWT(x,majorPeakInfo)

# calculate background

backgr = baselineCorrectionCWT(x,peakWidth,lambda=lambda,differences=1)

# subtract background

corrected=x-backgr

# plot original spectrum

plot(xa,x,type='l',ylim=c(min(c(x,corrected)),max(c(x,corrected))),main="The background-correction result of Raman Spectra",xlab=expression("Wavenumber / cm"^-1),ylab="Raman Intensity/Arbitr. Units")

# mark peaks

points(xa[majorPeakInfo$peakIndex],x[majorPeakInfo$peakIndex])

# add background

lines(xa,backgr,lty=5)

# add corrected spectrum

lines(xa,corrected)

# put corrected spectrum in data.frame

result<- data.frame(xa=xa, corrected=corrected)

# compute output name by first splitting the input name at the dot
```

```r
        # and putting it together with a string added to the first part

        partFn<- unlist(strsplit(files[i],".",fixed=TRUE))

        newFn<- paste(partFn[1],addToFn,".",partFn[2],sep="")

        # write to file

        write.table(result, file=newFn, sep="\t", row.names=FALSE)

        print("file written")

        # done only once: get column names, i.e. central wavelengths of the major
peaks

        if(i == 1)

        {

                peakPos<- as.character(round(result[majorPeakInfo$peakIndex,1]))

        }

        spectrumPeakAreas<- c()

        spectrumPeakPos<- c()

        # cut out every single detected peak and fit with Lorentzian profile

        for(j in 2:length(names(peakWidth)))

        {

                # read out the leftmost and rightmost index of the respective peak

                peakRange<- range(peakWidth[[j]])

                # create "new" x- and y-axis vector and list containing both

                peakX<- result[peakRange[1]:peakRange[2],1]

                peakY<- result[peakRange[1]:peakRange[2],2]

                peakData<- list(x=peakX,y=peakY)

                # FWHM estimated as one fourth of the difference at the baseline

                paramS<- round((result[peakRange[2],1] - result[peakRange[1],1])/4)

                # intensity at center wavelength multiplied with 1.5 times the FWHM

                paramH<- round(abs(result[peakWidth[[1]][j-1],2])*paramS*3/4)


                # center wavelength

                paramM<- round(result[peakWidth[[1]][j-1],1])
```

```
                    print(paste(i," ",j,"/",length(names(peakWidth)),sep=""))

                    print(paste("s=",paramS,", h=",paramH,", m=",paramM,sep=""))

                    # do the fit with nonlinear least squares, central wavenumber has to be
read from the original data

                    lorentz<-          nls(y~h*s/(s^2+(x-m)^2),          data=peakData,
start=list(s=paramS,h=paramH,m=paramM),                                    trace=TRUE,
control=nls.control(maxiter=500))

                    print(summary(lorentz))

                    #

                    # linearisation and refinement of the x-axis

                    predX<-
seq(round(result[peakRange[1],1],digits=1),round(result[peakRange[2],1],digits=1),by=0.
1)

                    lorentz.pred = predict(lorentz, data.frame(x=predX))

                    lorentz.int = sum(lorentz.pred)*0.1

                    # remember peak areas and respective peak positions

                    spectrumPeakAreas<- c(spectrumPeakAreas, lorentz.int)

                    spectrumPeakPos<- c(spectrumPeakPos,paramM)

                    # add to plot

                    lines(predX,lorentz.pred,col=3)

              }

              # add to peakArea, peakAreaList (and peakPos if necessary)

              peakAreaList<-
c(peakAreaList,list(list(pos=spectrumPeakPos,area=spectrumPeakAreas)))

              #peakArea<- rbind(peakArea,t(spectrumPeakAreas))

       }

       # writepeakAreaList in file

       write("", file="peakAreaList.txt")

       sink(file="peakAreaList.txt", append=TRUE)

       print(peakAreaList)

       sink()

       # add statistics to peakArea, i.e. mean and std. deviation for each peak
```

```
#means <- colMeans(peakArea)

#stddev<- apply(peakArea,2,sd)

#stat <- rbind(t(means),t(stddev))

#peakArea<- rbind(peakArea,stat)

#rownames(peakArea) <- c(as.character(1:length(files)),"mean","sd")

#colnames(peakArea) <- peakPos

# writepeakArea in file, add statistics

#write.table(peakArea,      file="peakArea.txt",      sep="\t",      row.names=TRUE,
quote=FALSE)

}
```

6. References

[1]. M. D. Hager, P. Greil, C. Leyens, S. Van Der Zwaag, and U.S. Schubert. *Adv. Mater.* , **2010**, **22**: p. 5424-5430.

[2]. S.V.D. Zwaag, *Self-healing Materials. An Alternative Approach to 20 Centuries*. Materials Science. **2007**, Dordrecht, The Netherlands: Springer.

[3]. D. Döhler, P. Michael, and W. H. Binder, *Principles of Self-Healing Polymers*, in *Self-Healing Polymers*. **2013**, Wiley-VCH Verlag GmbH & Co. KGaA. p. 5-60.

[4]. S.K. Ghosh, *Self healing materials- Fundamentals, Design strategies, and applications*. **2009**: Wiley-Vch Verlag GmbH & Co, KGaA, Weinheim.

[5]. K. S. Toohey, N. R. Sottos, J. A. Lewis, and J. S. Moore. *Nat. Mater.*, **2007**, **6**: p. 581-585.

[6]. E.B. Murphy and F. Wudl. *Prog. Polym. Sci.* , **2010**, **35**(1-2): p. 223-251.

[7]. S. R. White, N. R. Sottos, P. H. Geubelle, J. S. Moore, M. R. Kessler, S. R. Sriram, E. N. Brown, and S. Viswanathan. *Nature* **2001**, **409**: p. 794- 797.

[8]. L. Zedler, M. D. Hager, U. S. Schubert, M. J. Harrington, M. Schmitt, J. Popp, and B. Dietzek. *Mater. Today*, **2014**, **17**(2): p. 57-69.

[9]. S. Bode, L. Zedler, F. H. Schacher, B. Dietzek, M. Schmitt, J. Popp, M. D. Hager, and U.S. Schubert. *Adv. Mater.*, **2013**, **25**(11): p. 1634-8.

[10]. S. Bode, R. K. Bose, S. Matthes, M. Ehrhardt, A. Seifert, F. H. Schacher, R. M. Paulus, S. Stumpf, B. Sandmann, J. Vitz, A. Winter, S. Hoeppener, S. J. Garcia, S. Spange, S. Van Der Zwaag, M. D. Hager, and U.S. Schubert. *Polym. Chem.*, **2013**, **4**: p. 4966-4973.

[11]. D. G. Barrett , D. E. Fullenkamp , L. He , N. Holten-Andersen , K. Y. C. Lee , and P.B. Messersmith. *Adv. Funct. Mater*, **2013**, **23**: p. 1111-1119.

[12]. M. J. Harrington, A. Masic, N. Holten-Andersen, J. H. Waite, and P. Fratzl. *Science*, **2010**, **328**: p. 216-220.

[13]. M. Krogsgaard, M. A. Behrens, J. S. Pedersen, and H. Birkedal. *Biomacromolecules*, **2013**, **14**: p. 297-301.

[14]. A. E. Hughes, I. S. Cole, T. H. Muster, and R.J. Varley. *NPG Asia Mater.*, **2010**, **2**(4): p. 143-151.

[15]. A. Garcia. *Fuel*, **2012**, **93**: p. 264-272.

[16]. J. Kötteritzsch, S. Stumpf, S. Hoeppener, J. Vitz, M. D. Hager, and U. S. Schubert. *Macromol. Chem. Phys.*, **2013**, **214**: p. 1636-1649.

[17]. S. Burattini, B. W. Greenland, D. Chappell, H. M. Colquhoun, and W. Hayes. *Chem. Soc. Rev.*, **2010**, **39**: p. 1973-1985.

[18]. N.B. Pramanik, D. S. Bag, S. Alam, G. B. Nando, and N.K. Singha. *J. Polym. Sci. A Polym. Chem.*, **2013**, **0**: p. 001-010.

[19]. D. Döhler, P. Michael, and W. H. Binder. *Macromolecules*, **2012**, **45**(8): p. 3335-3345.

[20]. T. A. Plaisted and S. Nemat-Nasser. *Acta Mater.* , **2007**, **55**: p. 5684-5696.

[21]. E. B. Murphy, E. Bolanos, C. Schaffner-Hamann, F. Wudl, S. R. Nutt, and M.L. Auad. *Macromolecules*, **2008**, **41**: p. 5203-5209.

[22]. S. H. Cho, S. R. White, and P.V. White. *Adv. Mater.*, **2009**, **21**: p. 645-649.

[23]. J. S. Park, T. Darlington, A. F. Starr, K. Takahashi, J. Riendeau, and H. T. Hahn. *Compos. Sci. Technol.*, **2010**, **70**: p. 2154-2159.

[24]. X. Chen, M. A. Dam, K. Ono, A. Mal, H. Shen, S. R. Nutt, K. Sheran, and F. Wudl. *Science*, **2002**, **295**: p. 1698-1702.

[25]. J. Canadell, H. Fischer, G. De Witt, and R. A. T. M. Van Benthem. *J. Polym Sci. , Part A: Polym. Chem.*, **2010**, **48**: p. 3456-3467.

[26]. S. Dirilikov and J.L. Koenig. *J. Raman Spectrosc.*, **1980**, **9**(3): p. 150-154.

[27]. R. T. Bailey, A. J. Hyde, and J.J. Kim. *Spectrochim. Acta*, **1974**, **30A**: p. 91-98.

[28]. D. L. Gerrard and W.F. Maddam. *Appl. Spectroc. Rev.*, **1986**, **22**: p. 251-334.

[29]. M. D. Chipara, M. Chipara, E. Shansky, and J. M. Zaleski. *Polym. Adv. Technol.*, **2009**, **20**: p. 427-431.

[30]. W. Li, Z. Jiang, Z. Yang, and N. Zhao. *PLOS ONE*, **2013**, **8**(11): p. 1-18.

[31]. Y. Yang, M. D. Lepech, E-H. Yang, and V. C. Li. *Cem. Concr. Res. *, **2009**, **39**: p. 382-390.

[32]. B. De Graef, W. De Windt, J. Dick, W. Verstrarte, and N.D. Belie. *Mater. Struct.*, **2005**, **38**: p. 875-882.

[33]. P. Ghosh, S. Mandal, B.D. Chattopadhyay, and S. Pal. *Cem. Concr. Res.*, **2005**, **35**: p. 1980-1983.

[34]. S. Ghosh, M. Biswas, B. D. Chattopadhyay, and S. Mandal. *Cem. Concr. Compos.*, **2009**, **31**: p. 93-98.

[35]. H. M. Jonkers. *HERON*, **2011**, **56**: p. 1-12.

[36]. Y. Zhang, L. Tao, S. Li, and Y. Wei. *Biomacromolecules*, **2011**, **12**: p. 2894-2901.

[37]. H. Lee, S. M. Dellatore, W. M. Miller, and P. B. Messersmith. *Science*, **2007**, **318**: p. 426-430.

[38]. H.M. Jonkers, *Book Chapter Self Healing Concrete - A biological Approach*, in *Self-healing Materials. An Alternative Approach to 20 Centuries*. **2007**, Springer.

[39]. Z. Yang, J. Hollar, X. He, X. Chen, and X. Shi. *Cem. Concr. Compos.*, **2011**, **33**: p. 506-512.

[40]. A. Garcia, E. Schlangen, M. Van De Ven, and Q. Liu. *Constr. Build. Mater. *, **2009**, **23**: p. 3175-3181.

[41]. Q. Liu, A. Garcia, E. Schlangen, and M.V.D. Ven. *Constr. Build. Mater.*, **2011**, **25**: p. 3746-3752.

[42]. R.N. Lumley. *Mater. Forum*, **2007**, **31**: p. 40-51.

[43]. J. D. Rule, N. R. Sottos, and S.R. White. *Polym. Chem.*, **2007**(48): p. 3520-3529.

[44]. S. M. Bleay, C. B. Loader, V. J. Hawyes, L. Humberstone, and P.T. Curtis. *Composites Part A*, **2001**, **32**: p. 1767-1776.

[45]. M. Motuku, U. K. Vaidya, and G.M. Janowski. *Smart Mater. Struct.*, **1999**, **8**: p. 623-638.

[46]. D.G. Shchukin. *Polym. Chem.*, **2013**(4): p. 4871-4877.

[47]. V. Amendola and M. Meneghetti. *J. Mater. Chem. *, **2012**, **22**: p. 24501-24508.

[48]. M. Zako and N. Takano. *J. Intell. Mater. Syst. Struct.*, **1999**, **10**: p. 836-841.

[49]. S. Billiet, X. K. D. Hillewaere, R. F. A. Teixeira, and F. E. Du Prez. *Macromol. Rapid Commun.*, **2013**, **34**: p. 290-309.

[50]. T. C. Mauldin and M. R. Kessler. *Int. Mater. Rev.*, **2010**, **55**(6): p. 317-346.

[51]. H. Zhang and J. Yang. *J. Mater. Chem. A*, **2013**, **1**: p. 12715-12720.

[52]. M. P. Stevens and A.D. Jenkins. *J. Polym. Sci., Part A: Polym. Chem. *, **1979**, **17**: p. 3675-3685.

[53]. F. Herbst, S. Seiffert, and W.H. Binder. *Polym. Chem.*, **2012**, **3**: p. 3084-3092.

[54]. D. C. Tuncaboylu, M. Sari, W. Oppermann, and O. Okay. *Macromolecules*, **2011**, **44**: p. 4997-5005.

[55]. S. J. Kalista Jr and T.C. Ward. *J. R. Soc. Interface*, **2007**, **4**: p. 405-411.

[56]. S. J. Kalista Jr, J. R. Pflug, and R.J. Varley. *Polym. Chem.*, **2013**, **4**: p. 4910-4926.

[57]. Y. Yang and M.W. Urban. *Chem. Soc. Rev.*, **2013**, **42**: p. 7446-7467.

[58]. R.P. Wool. *Macromolecules*, **1993**, **26**: p. 1564-1569.

[59]. M. Doi and S.F. Edwards. *J. Chem. Soc., Faraday Trans. 2*, **1978**, **74**: p. 1789-1801.

[60]. X. Chen, M. A. Dam, K. Ono, A. Mal, H. Shen, S. R. Nutt, K. Sheran, and F. Wudl. *Science*, **2002**, **295**(5560): p. 1698-702.

[61]. H. Weizman, C. Nielsen, O. S. Weizman, and S. Nemat-Nasser. *J. Chem. Educ.*, **2011**, **88**(8): p. 1137-1140.

[62]. M. Q. Zhang and M.Z. Rong. *Polym. Chem.*, **2013**, **4**: p. 4878-4884.

[63]. P. Cordier, F. Tournilhac, C. Soulie- Ziakovic, and L. Leibler. *Nat. Mater.*, **2008**, **451**: p. 977-980.

[64]. S. Burattini, H. M. Colquhoun, B. W. Greenland, and W. Hayes. *Farad. Discuss.*, **2009**, **143**: p. 251-264.

[65]. S. Burattini, H. M. Colquhoun, J. D. Fox, D. Friedmann, B. W. Greenland, P. J. F. Harris, W. Hayes, M. E. Mackay, and S.J. Rowan. *Chem. Commun.*, **2009**: p. 6717-6719.

[66]. H. C. Kolb, M. G. Finn, and K.B. Sharpless. *Angew. Chem. Int. Ed*, **2001**, **40**: p. 2004-2021.

[67]. R. Huisgen. *Angew. Chem. Int. Ed*, **1968**, **7**(5): p. 321-406.

[68]. V. V. Rostovtsev, L. G. Green, V. V. Forkin, and K.B. Sharpless. *Angew. Chem. Int. Ed*, **2002**, **41**(14): p. 2596-2599.

[69]. N. B. Pramanik, G. B. Nando, and N.K. Singha. *Polymer* **2015**, **xxx**: p. 1-8.

[70]. R. Huisgen. *Angew. Chem. Int. Ed*, **1963**, **2**(10): p. 565-632.

[71]. R. Huisgen. *Angew. Chem. Int. Ed*, **1963**, **2**(11): p. 633-696.

[72]. J. E. Moses and A.D. Moorhouse. *Chem. Soc. Rev.*, **2007**, **36**: p. 1249-1262.

[73]. C. W. Tornøe, C. Christensen, and M. Meldal. *J. Org. Chem.*, **2002**, **67**: p. 3057-3064.

[74]. J. Gierlich, G. A. Burley, P. M. E. Gramlich, D.M. Hammond, and T. Carell. *Org. Lett.*, **2006**, **8**(17): p. 3639-3642.

[75]. J.-F. Lutz. *Angew. Chem. Int. Ed*, **2008**, **47**: p. 2182-2184.

[76]. D. D. Diaz, K. Rajagopal, E. Strable, J. Schneider, and M. G. Finn. *Am. Chem. Soc.*, **2006**, **128**: p. 6056-6057.

[77]. H. Li, F. Cheng, A. M. Duft , and A. Adronov. *J. Am. Chem. Soc.*, **2005**, **127**: p. 14518-14524.

[78]. D. I. Rozkiewicz, D. Jan´Czewski, W. Verboom, B. J. Ravoo, and D.N. Reinhoudt. *Angew. Chem., Int. Ed.,*, **2006**, **45**: p. 5292-5296.

[79]. V. Ladmiral, G. Mantovani, G. J. Clarkson, S. Cauet, J. L. Irwin, and M. Haddleton. *J. Am. Chem. Soc.*, **2006**, **128**: p. 4823-4830.

[80]. V. V. Rostovtsev, L. G. Green, V. V. Fokin, and K. B. Sharpless. *Angew. Chem. Int. Ed.*, **2002**, **41**(14): p. 2596-2599.

[81]. W. H. Binder and R. Sachsenhofer. *Macromol. Rapid Commun.*, **2007**, **28**: p. 15-54.

[82]. M. Gragert, M. Schunack, and W. H. Binder. *Macromol. Rapid Commun.*, **2011**, **32**(5): p. 419-25.

[83]. M. Meldal and C.W. Tornøe. *Chem. Rev.*, **2008**, **108**: p. 2952–3015.

[84]. L. Liang and D. Astruc. *Coord. Chem. Rev.*, **2011**, **255**(23-24): p. 2933-2945.

[85]. M. Schunack, M. Gragert, D. Döhler, P.Michael, and W.H. Binder. *Macromol. Chem. Phys.*, **2012**, **213**(2): p. 205-214.

[86]. O. Diels and K. Alder. *Liebigs Ann.*, **1928**, **460**(1): p. 98–122,.

[87]. K. Maruoka, S. Saito, and H. Yamamoto. *J. Am. Chem. Soc.*, **1992**, **114**: p. 1089-1090.

[88]. G. N. Fickes and T.E. Metz. *J. Org. Chem.*, **1978**, **43**(21): p. 4057-4061.

[89]. I. Tabushi, K. Yamamura, Z. Yoshida, and A. Togashi. *Bull. Chem. Soc. Jpn.*, **1975**, **48**(10): p. 2922-2926.

[90].   F. Fringuelli and A. Taticchi, *The Diels-Alder Reaction :Selected Practical Methods* **2002**, England: John Wiley & Sons, Ltd.

[91].   H. S. Mosher and J.D. Morrison. *Science*, **1983**, **221**(4615): p. 1013-1019.

[92].   K. Maruoka , T. Itoh , T. Shirasaka , and H. Yamamoto. *J. Am. Chem. Soc.*, **1988**, **110**: p. 310–312.

[93].   Y. Chen and J.K. Snyder. *Tetrahedron Lett.*, **1997**, **38**(9): p. 1477-1480.

[94].   C.V. Raman. *Indian J. Phys*, **1928**, **2**: p. 399-419.

[95].   M. Amiji, T. Chernenko, D. Cialla, T. Dieing, M. Dienm, B. Dietzek, M. Fries, N. Gierlinger, T. F. Haefele, O. Hollricher, W. Ibach, A. Jungen, A. Kale, J. Koenen, C. Mattäus, L. Milane, M. Milikovic, J. Müller, K. Paulus, J. Popp, L. Quintero, U. Schmidt, M. Schmitt, R. Spolenak, A. Steele, V. Torchilin, T. Wermelinger, and K. Wormuth, *Confocal Raman Microscopy*. Springer Series in OPTICAL SCIENCES. **2010**.

[96].   D.A. Long, *The Raman Effect: A unified treatment of the Theory of Raman Scattering by Molecules*. **2002**, England: John Wiley & Sons Ltd.

[97].   E. Smith and G. Dent, *Modern Raman Spectroscopy- A modern approach*. **2005**: John Wiley & Sons Ltd.

[98].   M. Schmitt and J. Popp. *J. Raman Spectrosc.*, **2006**, **37**: p. 20-28.

[99].   J.L. Koenig. *Appl. Spectroc. Rev.*, **1971**, **4**: p. 233-305.

[100].   M. Pigeon, R. E. Prud'homme, and M. Pezolet. *Macromolecules*, **1991**, **24**.

[101].   C. C. Naylor, R. J. Meier, B. J. Kip, K. P. J. Williams, S. M. Masnson, N. Conroy, and D.L. Gerrard. *Macromolecules*, **1995**, **28**: p. 2969-2978.

[102].   H. J. Bowley, D. L. Gerrard, W. F. Maddams, and M.R. Paton. *Makromol. Chem.*, **1985**, **186**: p. 695-705.

[103].   H. J. Bowley, D. L. Gerrard, and W. F. Maddams. *Makromol. Chem.*, **1985**, **186**: p. 707-714.

[104].   A. C. Angood and J.L. Koenig. *J. Macromol. Sci.-Phys.*, **1969**, **B3(2)**: p. 321-328.

[105].   Z.-M. Zhang, S. Chen, Yi-Z. Liang, Z.-X. Liu, Qi-M. Zhang, Li-Xia Ding, F. Ye, and H. Zhou. *J. Raman Spectrosc.*, **2010**, **41**: p. 659-669.

[106].   A. Savitzky and M.J.E. Golay. *Anal. Chem.*, **1964**, **36**(8): p. 1627-1639.

[107].   *Linkam Scientific Instruments*.

[108].   M. J. Frisch, G. W. Trucks, H. B. Schlegel, G. E. Scuseria, M. A. Robb, J. R. Cheeseman, G. Scalmani, V. Barone, B. Mennucci, G. A. Petersson, H. Nakatsuji, M. Caricato, X. Li, H. P. Hratchian, A. F. Izmaylov, J. Bloino, G. Zheng, J. L. Sonnenberg, M. Hada., M. Ehara, K. Toyota, R. Fukuda, J. Hasegawa, M. Ishida, T. Nakajima, Y. Honda, O. Kitao, H. Nakai, T. Vreven, J.A. Jr. Montgomery, J. E. Peralta, F. Ogliaro, M. Bearpark, J. J. Heyd, E. Brothers, K. N. Kudin, V. N. Staroverov, R. Kobayashi, J. Normand, K. Raghavachari., A. Rendell, J. C. Burant, S. S. Iyengar, J. Tomasi, M. Cossi, N. Rega, J. M. Millam, M. Klene, J. E.Knox, J. B. Cross, V. Bakken, C. Adamo, J. Jaramillo, R. E. Gomperts, O. Stratmann, A. J. Yazyev, R. Austin, C. Cammi, J. W. Pomelli, R. Ochterski, R. L. Martin, K. Morokuma, V. G. Zakrzewski, G. A. Voth, P. Salvador, J. J. Dannenberg, S. Dapprich, A. D. Daniels, O. Farkas, J. B. Foresman, J. V. Ortiz, J. Cioslowski, and D. J. Fox. **2009**.

[109].   A. D. Becke. *Phys. Rev. A: At. Mol. Opt. Phys.* , **1988**, **38**: p. 3098-3100.

[110].   B. Mielich, A. Savin, H. Stoll, and H. Preuss. *Chem. Phys. Lett.*, **1989**, **Volume 157**(3): p. 200-206.

[111].   C. Lee, W. Yang, and R. G. Parr. *Phys. Rev. B: Condens. Matter*, **1988**, **37**(2): p. 785-789.

[112].   T. Yanai, D. P. Tew, and N. C. Handy *Chem. Phys. Lett.*, **2004**, **393**: p. 51-57.

[113]. K. Burke, J. P. Perdew, and M. Ernzerhof, *Mixing Exact Exchange with GGA: When to Say When*, in *Electronic Density Functional Theory*, J. Dobson, G. Vignale, and M. Das, Editors. **1998**, Springer US. p. 57-68.

[114]. J. P. Perdew, J. A. Chevary, S.H. Vosko, K. A. Jackson, M. R. Pederson , D. J. Singh, and C. Fiolhais. *Phys. Rev. B*, **1992**, **46**(11): p. 6671-6687.

[115]. J. P. Perdew, J. A. Chevary, S.H. Vosko, K. A. Jackson, M. R. Pederson , D. J. Singh, and C. Fiolhais. *Phys. Rev. B*, **1992**, **46**: p. 4978.

[116]. R. Ditchfield, W. J. Hehre, and J. A. Pople. *J. Chem. Phys*, **1971**, **54**(724): p. 724-728.

[117]. A. D. Mclean and G. S. Chandler. *J. Chem. Phys.*, **1980**, **72**(5639): p. 5639-5648.

[118]. R. Krishnan, J. S. Binkley, R. Seeger, and J. A. Pople. *J. Chem. Phys*, **1980**, **72**: p. 650-654.

[119]. M. J. Frisch, J. A. Pople, and J. S. Binkley. *J. Chem. Phys*, **1984**, **80**: p. 3265-3269.

[120]. T. Clark, J. Chandrasekhar, G. W. Spitznagel, and P. Von Rague Schleyer. *J. Comput. Chem.*, **1983**, **4**(3): p. 294-301.

[121]. T. H. Dunning Jr. *J. Chem. Phys.*, **1989**, **90**(2): p. 1007-1023.

[122]. R. A. Kendall, T. H. Dunning Jr., and R. J. Harrison. *J. Chem. Phys*, **1992**, **96**: p. 6798-6806.

[123]. D. E. Woon and T. H. Dunning Jr. *J. Chem. Phys.*, **1993**, **98**(1358): p. 1358-1371.

[124]. J. P. Merrick, D. Moran, and L. Radom. *J. Phys. Chem. A*, **2007**, **111**: p. 11683-11700.

[125]. M. Wouters, E. Craenmehr, K. Tempelaars, H. Fischer, N. Stroeks, and J. Van Zanten. *Prog. Org. Coat.*, **2009**, **64**: p. 156-162.

[126]. S. Vasiliu, B. Kampe, F. Theil, B. Dietzek, D. Dohler, P. Michael, W. H. Binder, and J. Popp. *Appl. Spectrosc.*, **2014**, **68**(5): p. 541-8.

[127]. S. Sun and P. Wu. *J. Phys. Chem. A*, **2010**, **114**(32): p. 8331-8336.

[128]. H. Yamakoshi, K. Dodo, M. Okada, J. Ando, A. Palonpon, K. Fujita, S. Kawata, and M. Sodeoka. *J. Am. Chem. Soc*, **2011**, **133**: p. 6102-6105.

[129]. T. Weeks, S. Wachsmann-Hogiu, and T. Huser. *Opt. Express*, **2009**, **17**(19): p. 17044-17051.

[130]. P.L. Stanghellini and R. Rossetti. *Inorg Chem*, **1990**, **29**(11): p. 2047-2052.

[131]. J.C.O.a.J.S. J.F.Arenas. *J. Mol. Struct.*, **1993**, **294**: p. 45-48.

[132]. H.M. Badawi. *Journal of Molecular Structure (Teochem)*, **2002**, **583**: p. 89-97.

[133]. H.M. Badawi. *Journal of Molecular Structure*, **2008**, **888**: p. 379-385.

[134]. W.F. H.M. Badawi, K.S. Al-Ghamdi. *Journal of Molecular Structure*, **2003**, **624**: p. 225-232.

[135]. S. Mohan , K.S.P. Durairaj, and S.P. Jose. *Spectrochim. Acta, Part A*, **2003**, **59**: p. 1697-1704.

[136]. R.V. M. G. Samant, H. Seki, P. S. Bagus, C. J. Nelin, and M. R. Philpott. *J. Chem. Phys.*, **1988**, **89**(1): p. 583-589.

[137]. Z. Iqbal, W. Garrett, C. W. Brown, and S.S. Mitra. *J. Chem. Phys.*, **1971**, **55**: p. 4528-4535.

[138]. R.T. Lamoureux and D.A. Dows. *Spectrochim. Acta*, **1975**, **31A**: p. 1945-1949.

[139]. H. F. Shurvell and D.W. Hyslop. *J. Chem. Phys.*, **1970**, **52**: p. 881-887.

[140]. S.A. Medvedev, T. Palasyuk, I.A. Trojan, P.G. Naumov, J. Evers, T.M. Klapötke, and M.I. Eremets. *Vib. Spectrosc* **2012**, **58**: p. 188-192.

[141]. G.-C. Guo, W. Q.-M, and T.C.W. Mak. *J. Chem. Crystallogr.*, **1999**, **29**(5): p. 561-564.

[142]. D. Bougeard, N. Le Calve, B. Saint Roch, and A. Novak. *J. Chem. Phys.*, **1975**, **64**(12): p. 5152-5164.

[143]. V. Krishnakumar and R.J. Xavier. *Spectrochim. Acta, Part A*, **2004**, **60**: p. 709-714.

[144]. B. K. Yoo and S.-W. Joo. *J. Colloid Interface Sci.*, **2007**, **311**: p. 491-496.

[145]. A. A. Jbarah, A. Ihle, K. Banert, and R. Holze. *J. Raman Spectrosc.*, **2006**, **37**(1-3): p. 123-131.

[146]. H. Tabata, M. Fujii, S. Hayashi, T. Doi, and T. Wakabayashi. *Carbon*, **2006**, **44**(15): p. 3168-3176.

[147]. M. J. Taylor, D. S. Bohle, and S. Riethmiller. *J. Raman Spectrosc.*, **1984**, **15**(6): p. 393-395.

[148]. S. Lal and S. Diez-Gonzalez. *J. Org. Chem.*, **2011**, **76**(7): p. 2367-73.

[149]. P.J. Gemperline, *Practical guide to chemometrics- Principal Component Analysis*, in *Principal Component Analisys*, P. Gemperline, Editor. **2006**, Taylor & Francis Group, LLC. p. 69-105.

[150]. J. Zhou, N.K. Guimard, A. J. Inglis, M. Namazian, C.Y. Lin, M. L. Coote, E. Spyrou, S. Hilf, F. G. Schmidt, and C. Barner-Kowollik. *Polym. Chem.* , **2012**, **3**: p. 628-639.

[151]. C. Toncelli, D. C. De Reus, F. Picchioni, and A. A. Broekhuis. *Macromol. Chem. Phys.*, **2012**, **213**(2): p. 157-165.

[152]. A. M. Peterson, R. E. Jensen, and G. R. Palmese. *ACS Appl. Mater. Interfaces*, **2010**, **2**(4): p. 1141-9.

[153]. P. Reutenauer, E. Buhler, P. J. Boul, S. J. Candau, and J. -M. Lehn. *Chem. Eur. J.*, **2009**, **15**: p. 1893-1900.

[154]. L. W. Pickett. *J. Chem. Phys*, **1942**, **10**: p. 660-663.

[155]. M. Rico, M. Barrachina, and J. M. Orza. *J. Mol. Spectrosc.* , **1967**, **24**: p. 133-148.

[156]. Y. T. Lee, S. L. Wallen, and J. Jonas. *J. Phys. Chem.* , **1992**, **96**: p. 4282-4288.

[157]. T. D. Klots, R. D. Chirico, and W. V. Steele. *Spectrochim. Acta*, **1994**, **50A**(4): p. 765-795.

[158]. T. Kim, R. S. Assary, L. A. Curtiss, C. L. Marshall, and P. C. Stair. *J. Raman Spectrosc.*, **2011**, **42**(12): p. 2069-2076.

[159]. E. C. Aguiar, J. B. P. Da Silva, and M. N. Ramos. *Spectrochim. Acta A Mol. Biomol. Spectrosc.*, **2008**, **71**(1): p. 5-9.

[160]. T. Woldbaek, P. Klaboe, and C. J. Nielsen. *J. Mol. Struct.*, **1975**, **27**: p. 283-301.

[161]. A. J. Barnes, L. Le Gall, C. Madec, and J. Lauransan. *J. Mol. Struct.*, **1977**, **38**: p. 109-120.

[162]. M. Karabacak, A. Çoruh, and M. Kurt. *J. Mol. Struct.*, **2008**, **892**(1-3): p. 125-131.

[163]. S.- W. Joo. *Bull. Korean Chem. Soc.*, **2008**, **29**(9): p. 1761-1764.

[164]. J. R. Quinan and S. E. Wiberley. *Anal. Chem.*, **1954**, **26**(11): p. 1762-1764.

[165]. Y. C. Yuan, T. Yin, M. Z. Rong, and M. Q. Zhang. *eXPRESS Polym. Lett.*, **2008**, **2**(4): p. 238-250.

[166]. J. R. Quinan and S.E. Wiberley. *Anal. Chem.*, **1954**, **26**(11): p. 1762-1764.

[167]. S. Garasevych, M. Iakhnenko, O. Slobodyanyuk, and I. Vaskivskyi. *J. Spectrosc.*, **2010**, **24**: p. 191-195.

[168]. J. Lokaj, P. Vicek, and J. Kriz. *J. Appl. Polym. Sci.*, **1998**, **74**: p. 2378-2385.

[169]. E. Gulari, K. Mckeigue, and K.Y.S. Ng. *Macromolecules*, **1984**, **17**: p. 1822-1825.

Acknowledgements

First and foremost, I would like to thank to Prof. Dr. Jürgen Popp for this great opportunity of joining this work group, and being member of an experienced team in the domain of Raman spectroscopy. Without his supervision and help my work would not have been possible. His guidance was irreplaceable during this journey. I sincerely thank him for all of his help. Also, I would like to thank to Prof. Dr. Michael Schmitt for all the help and careful advices during my work.

I would like to thank Prof. Dr. Benjamin Dietzek. Always ready to make sure that I remained focused on the important details instead of future problems, he helped me not only to finish this degree, but provided several lessons of life as well.

My grateful thoughts are going to my colleagues for their understanding and helpful advices Dr. Martin Schulz for constant supervision of my chemistry knowledge, Dr. Frank Theil for the DFT calculations but mostly for the deeper understanding of software details used in my work, Dr. Nicolae Tarcea for making communication the easiest and most efficient way to focus and work, and Bernd Kampe for his computational contributions.

Many thanks for their support, help and creating a friendly environment, to my office colleagues Dr. Paul-Ernesto Vargas-Jentzsch and Dragana Kusic.

My sincere thanks to our partners, Institute of Chemistry, Division of Technical and Macromolecular Chemistry, Halle University, Germany, Prof. Dr. W. Binder , Diana Döhler, Philipp Michael, Halle University, Germany that provided us with chemical samples, as well with constant ideas exchange, in the case of the azide-alkyne reaction studies. This work was supported by the DFG Priority Programme "Design and Generic Principles of Self-healing Materials" (SPP 1568), project BI 1337/8-1 (WHB, PM, DD).

As well special thanks for the fruitful collaboration with the IOMC JENA- Laboratory for Organic and Macromolecular Chemistry, UNI Jena- IOMC, AG. Schubert, Prof. Dr. U. Schubert, Dr. Martin Hager, Julia Kötteritzsch for providing us with the samples for the Diels-Alder cycloaddition, but also for the countless meetings we spent while finding solutions and establishing future strategies for our experiments. This work was supported by the DFG Priority Programme "Design and Generic Principles of Self-healing Materials" (SPP 1568), projects SCHU1229/13-1 and PO563/25-2.

To my family, my parents Niculina and Laurențiu, my brother Andrei and my close friends, I am grateful for their constant support, encouragement and inspiration.

Curriculum Vitae

Personal Info

Name	Simona Vasiliu
Birthdate	06.03.1986
Birthplace	Vatra-Dornei, Romania

Education

2001-2005	Theoretical high-school „Ion-Luca", Vatra-Dornei, Romania
10/2005-07/2008	*Babes-Bolyai University*, Cluj-Napoca, Romania **B.Sc. (Physics)**, *Faculty of Physics* Thesis topic : „Detection of water pollutants by means of Surface Enhanced Raman Spectroscopy",,
10/2009-03/2010	*Friedrich Schiller University*, Institute of Physical Chemistry, Jena Erasmus-Student: experimental work for master thesis „Fabrication and UV-VIS assessment of nanostructured thin films based on TiO_2 and Au particles"
10/2008-02/2011	*Babes-Bolyai University*, Cluj-Napoca, Romania **M.Sc.**, *Faculty of Physics* Science and Technology for Advanced Materials Thesis topic : „Fabrication and UV-VIS assessment of nanostructured thin films based on TiO_2 and Au particles"
10/2008-06/2011	*Babes-Bolyai University*, Cluj-Napoca, Romania **M.Sc.**, *Faculty of Environmental Science and Engineering* Thesis topic : „TiO_2 as a material for fotocatalysis"
08/2011-current	*Friedrich Schiller University* Jena, Germany **Ph.D.**, Institute of Physical Chemistry, Leibniz Institute of Photonic Technologies Jena e.V. Thesis topic: „ Raman Characterization of Polymer Formation - First Step to Self-Healing Polymer Coatings Studies-"

Work Experience

08/2011-12/2014	Researcher, Friedrich Schiller University, Institute of Physical Chemistry, Jena

Declaration of originality

Selbstständigkeitserklärung:

Ich erkläre, dass ich die vorliegende Arbeit selbständig und unter Verwendung der angegebenen Hilfmittel, persönlichen Mitteilungen und Quellen angefertigt habe.

Jena, den

Simona Vasiliu